Biol. Cybern. 86, 191–207 (2002)
DOI 10.1007/s00422-001-0289-7

Biological Cybernetics

Theoretical considerations on canal–otolith interaction and an observer model

Jelte E. Bos, Willem Bles

TNO Human Factors, P.O. Box 23, 3769 ZG Soesterberg, The Netherlands

Received: 11 May 2001 / Accepted in revised form: 27 September 2001

Abstract. Subjective vertical orientation, eye and body movements, and motion sickness all depend on the way our central nervous system deals with the gravito-inertial force resolution problem: how to discern accelerations due to motion from those due to gravity, despite these accelerations being physically indistinguishable. To control body or eye movements, the accelerations due to motion should be known explicitly. Hence, somehow gravity should be filtered out of the specific force or gravito-inertial acceleration (GIA, the sum of both accelerations) as sensed by the otoliths, which are the linear accelerometers in the inner ear. As the GIA also changes in a head-fixed frame of reference when the head is rotated, angular motion as sensed by the semicircular canals in the inner ear should also be considered. We present here a theoretical approach to this problem, and show that the mathematical description of canal–otolith interaction is in fact a three-dimensional equivalent of the two-dimensional description given by Mayne in 1974. A simple low-pass filter is used to divide the GIA into a motion and a gravity component. The retardation of the somatogravic effect by concomitant angular motion during centrifugation is shown as a result. Furthermore we show how the canal–otolith interaction fits within the framework of an observer model to describe subjective vertical orientation, eye movement and motion sickness characteristics. To predict a frequency peak in sickness severity, for example, it is necessary to explicitly include the Mayne equation operating both on sensor afferents *and* in the internal model. From tilt and translation data from centrifugation and horizontal oscillation, as well as from motion sickness data, we conclude that the time constant of the low-pass filter is in the order of seconds instead of tens of seconds as assumed before. Several corollaries are additionally discussed as a result.

Correspondence to: J. E. Bos
(Tel.: +31-346-356371, Fax: +31-346-353977
e-mail: Bos@tm.tno.nl)

1 Introduction

Previously we introduced a model to explain and quantitatively predict motion sickness (Bos and Bles 1998). This model is based on the assumption that motion sickness is the result of a discrepancy between the gravitational vertical, as determined by integrated sensory information, and a vertical as expected based on previous experience (see also Bles et al. 1998, 2000). This model is shown schematically in Fig. 1.

Basically, this observer model describes the control of body motion. A desired body state $\boldsymbol{u}_d$ directs a controller (C) generating motor commands ($\boldsymbol{m}$) that subsequently drive the muscles in our body to fulfil the desire. With additional external perturbations (text in Fig. 1, e.g. by a car, ship or aeroplane), this results in the actual body state ($\boldsymbol{u}$). This state is sensed by somatosensory, visual and vestibular sensors (S) which, together with some central nervous system (CNS) processing and delay, results in afferent signals representing the state of the body ($\boldsymbol{u}_s$). Parallel to this primary path of signal flow, akin afferents are supposed to be generated by a copy of the primary path ($\hat{\mathbf{B}}$ and $\hat{\mathbf{S}}$), together called an internal model or neural store, and is supposed to be created by previous experiences. The input of this internal model is a copy of the motor commands that is also called an efference copy or corollary discharge. Here the output $\hat{\boldsymbol{u}}$ should be a better estimate of the body state as compared to the output $\boldsymbol{u}_s$ (this will be explained later), and it is this estimate that is compared with the desired state $\boldsymbol{u}_d$ to generate the error signal ($\boldsymbol{e}$). Optimally, the output of the internal model $\hat{u}_s$ should be equal to that of the primary path $\boldsymbol{u}_s$. If, for example, an external perturbation is present, these afferents will not be equal. The difference $\boldsymbol{u}_s - \hat{\boldsymbol{u}}_s$ or conflict ($\boldsymbol{c}$) may then give rise to an additional feedback signal, weighted by $\mathbf{K}$, and used by the internal model to drive the difference towards zero. Now the body state $\boldsymbol{u}$ has several components, e.g. angular velocity, linear acceleration and gravity. Oman (1982) suggested that the resulting multi-vectorial conflict is correlated with motion sickness (s) as postulated by Reason and Brand (1975). It can, however, be shown

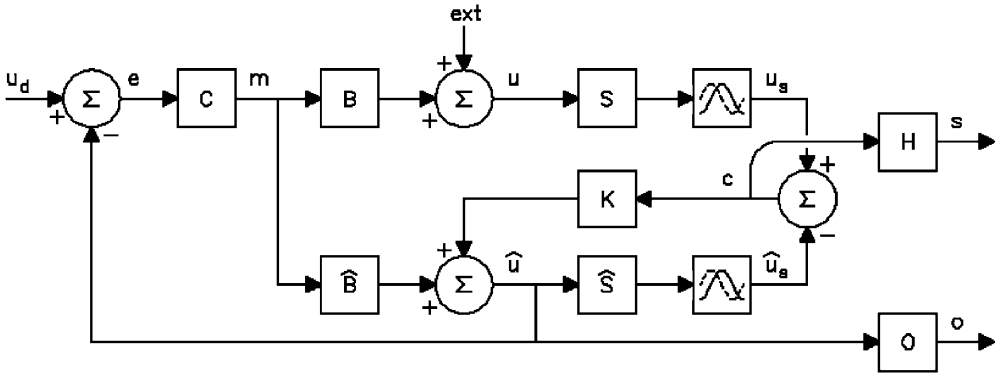

Fig. 1. Spatial orientation and motion sickness model (see text for details)

that with only the difference between the gravity components, motion sickness can successfully be predicted as it has been observed in a quantitative way (see Bos and Bles 1998, and below).

The same model approach has been used to explain the behaviour of psychophysical responses (o) like the subjective vertical (Glasauer 1992a; Glasauer and Merfeld 1997), as well as physiological responses such as eye movements (Merfeld et al. 1993). These similarities make sense, because the main output of the model of Fig. 1 ($\hat{\boldsymbol{u}}$) is a sense of self-motion, and eye movements should oppose self-motion when a stable retinal image of the outer world is required (the vestibulo-ocular reflex). However, there are several aspects that have not been made clear yet. Predictions of additional models presented so far are most often one dimensional, the interaction between canals and otoliths in these models has not been resolved unambiguously, the role of gravity has often been smuggled, it is unclear whether we need an internal model anyway and there is a need for unification in regard to the variety of models (e.g. Young and Meiry 1968; Mayne 1974; Mittelstaedt 1975, 1983; Borah et al. 1988; Droulez and Darlot 1989; Viéville and Faugeras 1990; Glasauer 1992b,c; Bles and de Graaf 1993; Angelaki and Hess 1996a,b, 1999; Telford et al. 1997; Seidman et al. 1998; Crane and Demer 1999; Mergner and Glasauer 1999). This paper is therefore meant to further clarify these matters in a theoretical and mathematical sense.

Because the three-dimensional characteristics of eye movements have been particularly popular in the literature of the last decade, we will not go into these responses in detail. Though vision and somatosensory cues are important, the points we want to raise can be dealt with by primarily considering the vestibular system, and for reasons of simplicity we will furthermore limit this paper mostly to vestibular cues. The gravito-inertial force (GIF) resolution now becomes a major problem to be solved within the sensor blocks S and $\hat{S}$ of Fig. 1. Accelerations due to motion and gravity are physically equivalent, but for proper control of body motion, only the accelerations due to motion should be known. This will be dealt with in Sect. 2. Section 3 will then discuss how our CNS may solve the GIF-resolution problem when both angular and linear motion are at stake (a further elaboration of the sensor function S in Fig. 1).

Sections 2 and 3 together describe the basic canal–otolith interaction that runs as a thread through this paper. Section 4 will focus on *why* we need internal models, and presents some possibilities on *how* to integrate the findings obtained so far. But, only one of these possibilities invitingly suits the explanation of certain motion sickness characteristics, and this closes the circle started here in this section. In addition, we will summarise and present some essential facts, novel explanations and observations throughout the text by means of intermezzos, while the majority of mathematical derivations will be given in appendices.

2 GIF resolution

To be able to move about on earth in a controlled manner requires knowledge of self-motion. This holds for linear as well as angular motion, both with three Cartesian components. On earth we are also faced with gravity, and a total of nine variables must therefore be considered. Physically, however, accelerations due to motion and due to gravity are indistinguishable, a fact also referred to as Einstein's equivalence principle, or the GIF-resolution problem (cf. Merfeld 1995).

Intermezzo: Motion and gravity. By Newton's second law we know that a mass m moved with an acceleration $\boldsymbol{a} = \mathrm{d}^2\boldsymbol{x}/\mathrm{d}t^2$ (with $\boldsymbol{x}$ representing position) is subject to a force $\boldsymbol{F} = m\boldsymbol{a}$, or any mass m to which a force $\boldsymbol{F}$ is applied tends to move with an acceleration $\boldsymbol{a}$ (and hence, the ratio $\boldsymbol{F}/\boldsymbol{a}$ is a constant m). If two masses are involved (e.g. one being yourself and the other being the huge mass of earth), these will attract each other with a force proportional to both these masses (Newton's gravitational law). As before, this force provokes an acceleration specifically denoted by $\boldsymbol{g}$. So, when moving on earth we only "feel" the resultant of these accelerations, $\boldsymbol{f} = \boldsymbol{a} + \boldsymbol{g}$, where the specific force $\boldsymbol{f}$ is also called the gravito-inertial acceleration (GIA)[1]. To distinguish between $\boldsymbol{a}$ and $\boldsymbol{g}$, angular information is essential too, because head tilt may result in a condition with an equal head-referenced GIA as compared to one of pure linear acceleration[2]. An example is shown in Fig. 2.

[1] Irrespective the fact that the rest of the paper will only deal with accelerations (see Appendix A), we will keep using the term GIF resolution (instead of GIA resolution) to conform with Merfeld (1995).

[2] Under natural conditions, however, head rotations are rarely pure rotational through the interaural center (e.g. Medendorp et al. 1998).

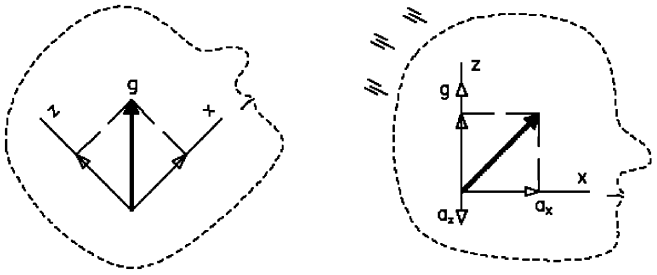

Fig. 2. By head rotation the GIA components may be as shown *left*. These GIA components may be exactly equal to those of a condition of combined forward (a_x) and downward (a_z) acceleration (such as during walking). For discerning these conditions, angular information is essential

By path integration we may calculate position[3] from acceleration. If we would then not discern gravity as such, we might feel like an astronaut within five minutes ($\Delta x = \iint g\,\mathrm{d}t^2 = 1/2gt^2 \approx 440$ km, with $g = 9.81$ m/s^2 and $\Delta t = 300$ s). Of course this is not the case, indicating that our CNS employs some algorithm to filter out gravity. An example regarding this peculiarity that is often overlooked in the literature on spatial orientation is given by the somatogravic effect (see the following intermezzos). The semicircular canals (SCC) are the part of the labyrinth in the inner ear that detects angular velocity ($\boldsymbol{\omega}$), and the otoliths are sensitive to the GIA (see Appendix A). The otoliths alone *cannot* make the distinction between rotation and linear acceleration, as is shown in Fig. 2. Moreover, because motion in the three-dimensional space should be described by six degrees of freedom (three rotational and three translational), both canal and otolith afferents are needed. For the CNS, the GIA is head referenced (the otoliths are head fixed), while gravity is earth fixed. Hence, the acceleration $\boldsymbol{a}$ needed for proper path integration should be calculated by

$$\boldsymbol{a} = \mathbf{R}_{\omega}(\boldsymbol{f}) - \boldsymbol{g} \tag{1}$$

Here, $\mathbf{R}_{\omega}$ represents the matrix determined by canal afferents ($\boldsymbol{\omega}$) to rotate the head-referenced GIA into an earth-referenced vector. It is essential that the rotation $\mathbf{R}$ is accurate (Viéville and Faugeras 1990; Mergner and Glasauer 1999), and perhaps more importantly, that gravity is known a priori. These two topics embody the key issue of the present paper, as described further in the remainder of this section.

Under natural conditions, i.e. of self-propelled (loco)motion, our vestibular system as a whole functions near perfection: we can control our body motion well (we rarely fall over), we can realise a satisfactory visual fixation and we do not get sick from motion. To this end we are equipped with sensors such as the eyes and a somatosensory and a vestibular system. It is only under artificial conditions such as being moved by a ship, or with incongruent vestibular and visual motion in a simulator, for example, that the system is driven beyond its range of near perfection and troubles with posture, gait, vision or sickness may occur. With advancing technology we are faced more and more with such unnatural conditions, therefore knowledge on canal–otolith interactions becomes even more relevant. In elaborating this interaction while focusing on the vestibular cues, often under unnatural conditions, the following imperfections are at stake. First, angular velocity is not sensed without errors by the SCC, e.g. there is no difference in the firing rate of SCC afferents between zero and constant angular velocity (see Appendix A, and the intermezzo on the Ferris wheel illusion in this section). Second, the assumption that our CNS "knows" $\boldsymbol{g}$ a priori is inappropriate. Both its magnitude and its orientation with respect to earth should then either be (genetically) predetermined or (more likely) set at conception, for example. Because sequences of DNA probably do not track orientation, an exclusive genetic origin can be ruled out. An initialisation at conception is also unlikely, since then it should be known by the impregnated cell that it is not moving with respect to earth, while its attitude has to be known. Hence knowledge (in a perceptual, and *not* in a cognitive sense) about gravity can only be gained during life, and due to the equivalence principle, filtering out gravity is a matter of inference, and not of physics. As a consequence, any model that relies on initial settings for motion and gravity therefore *cannot* represent the true function of our vestibular system.

The somatogravic effect and the Ferris wheel illusion may help better understand the way our CNS solves this GIF-resolution problem. Both effects concern our sense of verticality, or subjective vertical (SV), when only somatosensory and vestibular cues are at stake. We will therefore first consider the SV below.

Intermezzo: Subjective vertical. Most if not all living beings seem to experience a sense of verticality. Humans are fully aware of what is "up" and what is "down", even with the eyes closed (Bourdon 1906). It is not known *why* this is so and why the outer world is not perceived tilted or even inverted (Stratton 1896). We do know that several senses are involved. Vision is important, because trees and houses are naturally oriented vertically and their substrates are mostly horizontal, for example. Our vestibular system senses how we move and how we are oriented with respect to gravity. Somatosensory cues (e.g. ankle joints, abdominal graviceptors, neck muscle afferents and "seat of the pants"; see also Mittelstaedt and Fricke 1988; Mittelstaedt 1992) all typically point at the direction of the GIF. Depending on how it manifests itself, the perceived vertical (percept of $\boldsymbol{g}$) has been given various adjectives such as visual, kinaesthetic, postural, subjective, apparent or gravitational (Graybiel and Brown 1951; Gibson and Mowrer 1938; Gibson 1952, Mittelstaedt 1983, 1988). Here, we will use the term "sensed vertical" (denoted by $\tilde{\boldsymbol{g}}$) for the estimation of gravity as determined by our senses (see Fig. 1), and "subjective vertical" (denoted by $\hat{\boldsymbol{g}}$) when specifically the output of further processing by an internal model is meant. The abbreviation SV refers to any derivative of either the sensed or subjective vertical. Unfortunately, only these derivatives can be measured by verbal

[3] Position generally refers to translational position, whereas orientation refers to angular position. Attitude specifically refers to the angular orientation with respect to the earth perpendicular, or gravity.

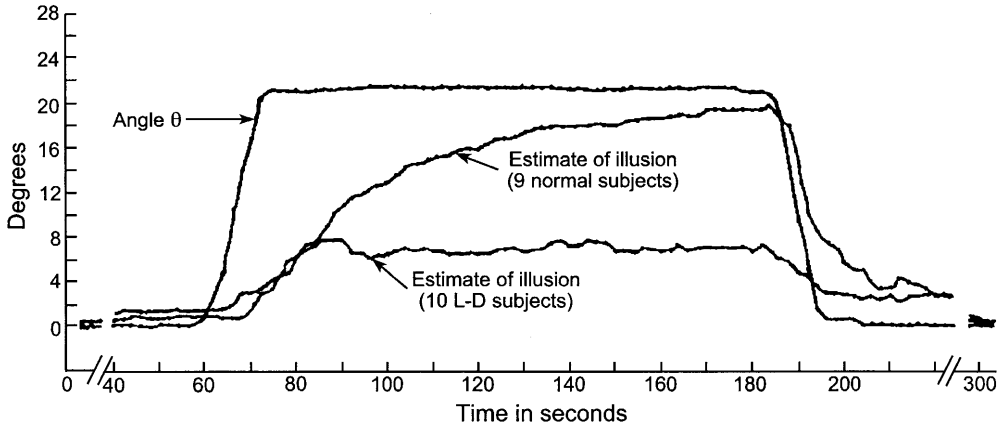

Fig. 3. Average estimated angle of tilt (θ) as observed by nine normal subjects and ten labyrinthine-defective (*L-D* subjects), experiencing a centripetal acceleration of approximately 0.4 g from $t = \pm 60$ s to $t = \pm 185$ s (after Graybiel and Clark 1965)

responses, joystick manipulations or adjustments of a visual line, for example. Albeit plausible, these derivatives (*o* in Fig. 1) do not necessarily correlate, due to their individual transfer functions (O).

Intermezzo: Somatogravic effect. The past two centuries have revealed many observations on *how* the SV behaves. Purkinje (1820) perceived a tilt during "centrifugation" in a merry-go-round, and Mach (1898) used a dedicated centrifuge and first observed a tilt asymmetry in response to acceleration and deceleration. Helmholtz (1866) also noticed that aboard a ship the cabin is seen stationary at first with a suspended barometer appearing to sway, whereas after a while the perceived vertical is "anchored to gravity" again. Wertheimer (1912) examined the tilt of this vertical induced by a tilted mirror image of the surroundings, indicating that verticality is attracted towards visual verticality within a period of minutes. Gibson and Mowrer (1938) lucidly reviewed a number of these examples. Temporal aspects became more clear with the advent of jet aircraft (Graybiel et al. 1947; Clark and Graybiel 1949) and the subsequent construction of high-G human centrifuges (Graybiel and Brown 1951; Clark and Graybiel 1963, 1966; Graybiel and Clark 1965). When a subject is fixed to the end of a centrifuge arm (a distance r from the centre) and he is rapidly brought to constant angular velocity (ω) about an earth vertical axis, he will experience a centripetal acceleration ($\omega^2 r$) which is perpendicular to the gravitational acceleration. The resultant GIA hence tilts ramp-wise with respect to the subject. It is observed that the SV only approaches the GIA asymptotically within a period of (tens of) seconds. This apparent tilt during centrifugation was termed the somatogravic (Graybiel et al. 1947) or oculogravic illusion, depending on whether it is perceived proprioceptively or visually (Graybiel and Clark 1965)[4,5]. Figure 3 shows some results of Graybiel and Clark (1965) on both healthy and labyrinthine defective subjects, indicating the significance of the vestibular apparatus regarding this effect. Observed time constants of the exponential increase range from 5 s to 20 s (Graybiel and Brown 1951; Clark and Graybiel 1963, 1966; Young and Meiry 1968; Stockwell and Guedry 1970; Guedry 1974; de Graaf et al. 1996; Seidman et al. 1998). Since Graybiel et al. (1947), some models on vestibular perception do employ these data (Mayne 1974; Glasauer 1992a,b; Bles and de Graaf 1993), and others do not (Merfeld et al. 1993; Angelaki et al. 1999; Droulez and Darlot 1989; Viéville and Faugeras 1990; Holly 1997). The somatogravic effect hence illustrates that we do *not* employ a veridical "sense" of verticality, but adapt to the GIA instead. The next sections will use this explicitly, giving a possible explanation for the large variability in time constants observed in terms of canal–otolith interactions, because in a centrifuge there is a concomitant angular signal.

Intermezzo: Ferris wheel illusion. When a subject is rotated with a constant angular velocity about an earth-horizontal axis, he will first perceive the veridical motion. But when his canal afferents have returned to their resting value (see Appendix A), normally corresponding to zero angular velocity, he will only feel a linear acceleration (Fig. 4). Because the horizontal component of this linear acceleration is 90° out-of-phase with the vertical component, and there is no canal angular velocity signal, this is interpreted as a circular motion with some fixed orientation (Mayne 1974; Mittelstaedt et al. 1989). This latter orientation is dependent upon path integration of canal afferents, the idiotropic vector (Mittelstaedt 1983) and somatosensory cues. For example, pressure applied to the feet will result in an upward orientation, while pressure applied to the head will result in an inverted orientation (J. E. Bos, W. Bles, Personal observation, 1988; Lackner and Graybiel 1978; Mittelstaedt et al. 1989). This illusion nicely shows the deficient functioning of our canal system under unnatural circumstances.

3 Canal–otolith interaction

Here, we will describe (conceptually and mathematically) the basic operations that should be realised to solve the GIF-resolution problem using otolith and canal afferents, and it will be shown that several models presented in the literature are, in fact, identical.

3.1 Basic considerations

Mayne already stated in 1974 that: "The processing of the otolith signals to separate the components due to

[4] Kornhuber (1974) makes a distinction between "proprioceptive" (concerning all registrations of motion and/or pressure), vestibular (the inner ear only) and somatosensory (all other motion and pressure) sensors. Defined this way, proprioception equals the sum of vestibular and somatosensory information. For this reason, we would now term the somatogravic effect as the proprioceptive effect instead. Nevertheless, we will keep to the classical term somatogravic effect in this paper.

[5] Such centrifuge experiments are applied in aviation to demonstrate the apparent tilt during a catapult launch from aircraft carriers, where pilots may experience a 3–5 g linear acceleration during take-off. If not reckoned, the ensuing illusory tilt may be (and has unawarely often been) compensated for by pitching down the plane, resulting in a controlled flight into the sea (see Cohen et al. 1973). Now that it is reckoned, aviators are trained to rely on their instruments, rather then on their "feelings".

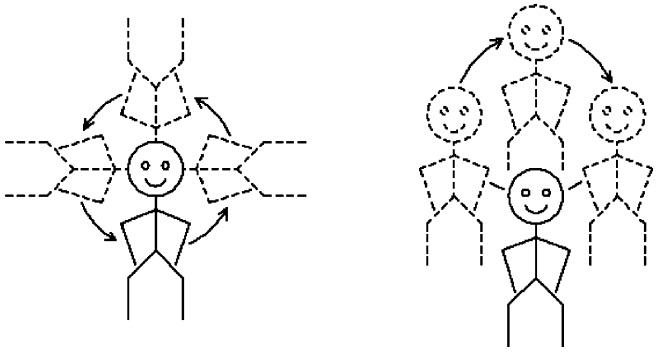

Fig. 4. Ferris wheel illusion. A subject rotating with a constant angular velocity about an earth-horizontal axis (*left*) perceives a motion like a gondola of a Ferris wheel after his canal signals have returned to their rest value (*right*)

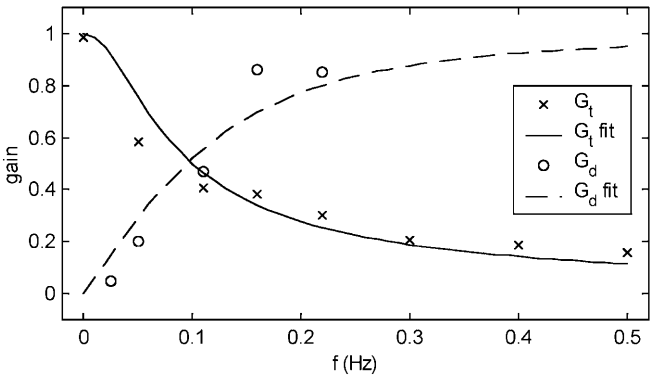

Fig. 5. Average tilt gains and displacement gains for different frequencies. Data are taken from de Graaf et al. (1996, 1998, and personal communication), and comprise centrifuge-only data ($f = 0$ Hz), centrifugation with concomitant translation ($f = 0.025, 0.05, 0.11$ Hz), and pure translation data ($f = 0.22, 0.3, 0.4, 0.5$ Hz)

gravity from those due to acceleration can only be based on one distinguishing characteristic, the constancy of one and the transient nature of the other. Gravity is identified by the system as the constant portion of the signal, acceleration as the transient portion'' (Mayne 1974; see also Viéville and Faugeras 1990 who, however, do not refer to Mayne). For normal human and animal (loco)motion, the accelerations encountered are always of short duration, or periodic, and this approach makes sense. Hence, if only linear accelerations are involved, three orthogonal systems with low-pass characteristics operating in an earth-fixed frame of reference can filter out gravity of the otolith afferents. Let us denote the percept of gravity by $\tilde{\boldsymbol{g}}$, indicate each Cartesian component with the index i and assume that the otolith output equals $\boldsymbol{f}$ (see Appendix A). These filters can then be represented either as ordinary differential equations or, equivalently in Laplace notation, with s as the complex frequency variable:

$$\frac{\mathrm{d}\tilde{g}_i}{\mathrm{d}t} = \frac{1}{\tau}(f_i - \tilde{g}_i) \quad \text{or} \quad \tilde{g}_i = \frac{1}{\tau s + 1} f_i \tag{2}$$

Then, analogous to (1), it should hold that

$$\tilde{\boldsymbol{a}} = \boldsymbol{f} - \tilde{\boldsymbol{g}} = \left(1 - \frac{1}{\tau s + 1}\right)\boldsymbol{f} = \frac{\tau s}{\tau s + 1}\boldsymbol{f} \tag{3}$$

where the otolith afferents are supposed to represent the GIA (Appendix A). Equation (3) implies that the acceleration of self-motion perception is just the opposite (i.e. a high-pass response) of the sensed vertical. The next intermezzo shows the validity of this assumption.

Intermezzo: Subjective tilt versus translation. De Graaf et al. (1996, 1998, and personal communication, 1994) recorded verbal estimations of tilt and translation during centrifugation at 0.5 g with and without a slowly varying arm length and during pure horizontal sinusoidal translation where only the distance travelled and the velocity were varied such that the peak acceleration was always 0.5 g. Translations were indicated by the subjects as the perceived distance travelled. Here we reanalysed the data of a total of 18 subjects as follows. From the tilt responses we calculated the hypothetical horizontal component $\tilde{g}_{\mathrm{hor}}$ of the SV, where $\tilde{g}_{\mathrm{hor}} = g_z \tan\theta$. Note that the SV, which may be tilted by an angle θ with respect to true verticality, is interpreted as the direction of gravity. We divided this value by the stimulus acceleration to obtain a tilt gain G_{t}. Displacement gains were calculated by dividing the perceived distance travelled by the actual distance travelled. Then, if these data were the result of simple first order low- and high-pass filtering of a sinusoidal input (a_{hor}) according (3), the tilt gains G_{t} and the displacement gains G_{d} would have to satisfy

$$G_{\mathrm{t}} = \left|\frac{\tilde{g}_{\mathrm{hor}}}{a_{\mathrm{hor}}}\right| = \sqrt{\frac{1}{1+\tau^2\omega^2}} \quad \text{and}$$
$$G_{\mathrm{d}} = \left|\frac{\tilde{a}_{\mathrm{hor}}}{a_{\mathrm{hor}}}\right| = \sqrt{\frac{\tau^2\omega^2}{1+\tau^2\omega^2}} \tag{4}$$

where we have used that for sinusoidal motion the peak acceleration equals displacement times ω^2 and hence displacement gain equals acceleration gain. Figure 5 shows the averages as observed and the fits according to (4). Here we found a time constant of 2.8 s for G_{t} and 1.0 s for G_{d}. Though these values are not equal, they are of the same order of magnitude, and much smaller than those observed in the somatogravic effect using centrifuges (see above). Therefore, this speaks in favour of a time constant of the low-pass filter in the order of seconds, instead of tens of seconds. The difference in time constants as inferred from Fig. 5 may be explained by an imperfect path integration. Irrespective of this difference, it is rewarding that indeed the perceived tilt behaves like a low-pass-filtered otolith response, while the distance travelled just shows the opposite behaviour as predicted.

If the head is rotated, the Cartesian components of the sensed (and thus head-referenced) GIA (or $\boldsymbol{f}_{\mathrm{h}}$, will change as shown in Fig. 2. Stockwell and Guedry (1970) have shown that if these motions are coplanar, the SV corresponds instantaneously with true verticality. Only if the otolith and canal inputs are dissociated, these authors argued, does this result in a delayed tilt sensation. This can be explained as follows. Because gravity is only constant relative to earth, the low-pass filtering to estimate $\boldsymbol{g}$ should accordingly be performed in an earth-fixed co-ordinate frame (cf. Eq. 1). Let now $\mathbf{R}_{\mathrm{h}}$ denote the rotation of the head, and $\boldsymbol{f}_{\mathrm{e}}$ the earth-referenced GIA, then $\boldsymbol{f}_{\mathrm{h}} = \mathbf{R}_{\mathrm{h}}^{-1}\boldsymbol{f}_{\mathrm{e}}$. For example, if the head rotates about an angle θ, the direction of an earth-referenced vector is rotated by $-\theta$ relative to the head.

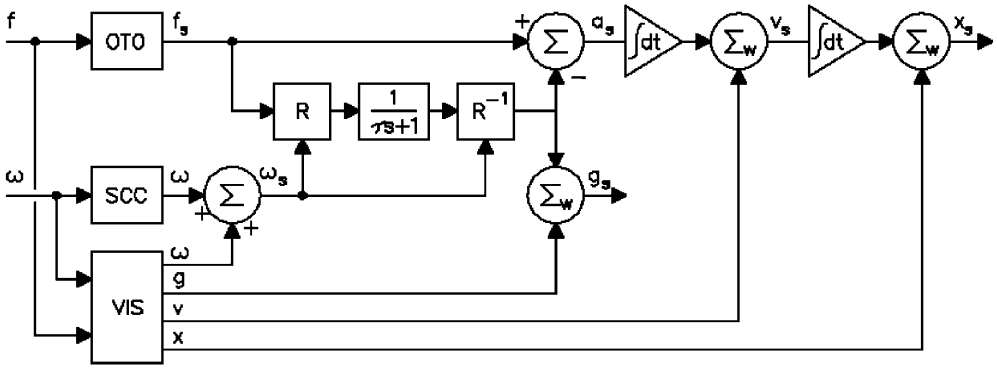

Fig. 6. Resolving the sensed angular velocity ($\boldsymbol{\omega}$), vertical ($\boldsymbol{g}_s$), and linear acceleration ($\boldsymbol{a}_s$), velocity ($\boldsymbol{v}_s$) and position ($\boldsymbol{x}_s$) by means of integrated otolith (OTO) canal (SCC) and visual (VIS) inputs (see text for further explanation)

Obviously, the SCC can supply this rotation information. If $\mathbf{R}_c$ represents the rotation matrix as determined by the canals, the estimate of the earth-referenced acceleration is given by $\boldsymbol{f}' = \mathbf{R}_c\mathbf{R}_h^{-1}\boldsymbol{f}_e$. In the ideal case, $\mathbf{R}_c = \mathbf{R}_h$ and $\boldsymbol{f}' = \boldsymbol{f}_e$. This, however, is not always so, such as under unnatural conditions of a Ferris wheel illusion. On the basis of this estimate of the earth-referenced GIA, the low-pass filtering can be performed, resulting in an earth-referenced $\tilde{\boldsymbol{g}}$. However, the estimate of gravity should be given in head-fixed coordinates, which can be realised by a second inverse rotation: $\tilde{\boldsymbol{g}}_h = \mathbf{R}_c^{-1}\tilde{\boldsymbol{g}}_e$. With $\mathbf{R} = \mathbf{R}_c$ these steps are visualised by the model of Fig. 6, an adapted version of the model introduced by Bles and de Graaf (1993) and Bles et al. (1998). Note that neither of these papers gives a comprehensive conceptual nor a mathematical explanation, and this section may be considered as compensating for this. In addition to vestibular inputs, Fig. 6 also postulates the integration of visual inputs. Because the stimulus for the vestibular apparatus equals that of the somatosensory system, at least up to the level of the head, the somatosensory signals are left out for reasons of simplicity. The visual system is supposed to divide its information into angular motion (optic flow, $\boldsymbol{\omega}$), attitude (i.e. orientation with respect to gravity, $\boldsymbol{g}$), linear velocity ($\boldsymbol{v}$) and position ($\boldsymbol{x}$). Because the visual system mainly responds to retinal scene position and velocity, and *not* to accelerations thereof, this information is merged only after the path integration of vestibular signals by some weighted averaging (cf. Howard 1997). Note that the weighting of visual frame information probably includes higher-order processes to explain the asymmetrical "righting" of the SV by the appearance and disappearance of a veridical "upright" visual scene (e.g. Mittelstaedt, 1988). This, however, falls beyond the scope of this paper. Because angular velocity from optic flow is here supposed to be a low-pass filtered response, whereas canal afferents are a high-pass response (Appendix A), an unweighted addition at this level suffices.

Analogous to the senses of verticality and motion as represented by (3), it has also been found that eye movements discriminate between motion and gravity. Translational responses typically show high-frequency characteristics, whereas tilt responses typically show low-frequency characteristics (e.g. Paige and Tomko 1991; Angelaki and Hess 1996a). This again suggests that both eye movements and psychophysical responses not only show similar behaviour, but may as well share the same mechanism as the one shown in Fig. 1. We will next examine mathematically the vestibular part of this concept.

3.2 Kinematics

In the model of Fig. 6, the reorientation matrix $\mathbf{R}$ is determined by angular velocity. This is generally considered to be a problem (i.e. it is not part of any standard textbooks on mathematical physics) for the following reason. Any rotation matrix is typically given by the direction cosines r_{ij} of the angles of the rotated axes relative to their origin, as in (5) below. However, rotations do not commute, and angles cannot be dealt with as vectors. Hence, the direction cosines cannot be obtained by direct vector integration of the angular velocities as provided by the canals. This problem can elegantly be solved using quaternions, so named by W.R. Hamilton in the nineteenth century, whose solution has been described by, for example, Westheimer (1957), Altmann (1986), and Tweed and Vilis (1987). Their results are combined and summarised in Appendix B. Consequently, the direction cosines r_{ij} from the rotation matrix $\mathbf{R}$ that rotates one vector $\boldsymbol{x}$ into its new coordinates $\boldsymbol{y}$:

$$\boldsymbol{y} = \mathbf{R}\boldsymbol{x} \quad \text{or} \quad \boldsymbol{x} = \mathbf{R}^{-1}\boldsymbol{y} \quad \text{with} \quad \mathbf{R} = \begin{pmatrix} r_{11} & r_{12} & r_{13} \\ r_{21} & r_{22} & r_{23} \\ r_{31} & r_{32} & r_{33} \end{pmatrix} \tag{5}$$

can be found by the angular velocity vector $\boldsymbol{\omega}$. Thus, if $\boldsymbol{\omega}$ is given by the canals, the sensed vertical can be determined by two successive rotations sandwiching the low-pass filter, as depicted in the centre of Fig. 6. This solution, however, requires four integrations (see Appendix B), a rather laborious determination of nine direction cosines, and two rotations.

Fortunately, there is an easier way to mathematically determine the sensed vertical from otolith and canal afferents ($\boldsymbol{f}$ and $\boldsymbol{\omega}$ respectively), and this alternative analysis will be presented here. As far as the vestibularly determined SV is concerned, the model from Fig. 6 can be reduced to that of Fig. 7. By (2) we have

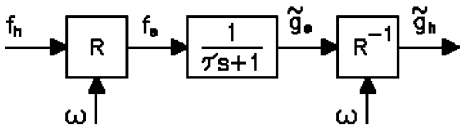

Fig. 7. Functional signal flow from head-referenced otolith ($\boldsymbol{f}_\mathrm{h}$) and canal ($\boldsymbol{\omega}$) afferents via earth-referenced afferents ($\boldsymbol{f}_\mathrm{e}$ and $\tilde{\boldsymbol{g}}_\mathrm{e}$) to the head-referenced sensed vertical ($\tilde{\boldsymbol{g}}_\mathrm{h}$)

$$\frac{\mathrm{d}\tilde{\boldsymbol{g}}_\mathrm{e}}{\mathrm{d}t} = \frac{1}{\tau}(\boldsymbol{f}_\mathrm{e} - \tilde{\boldsymbol{g}}_\mathrm{e}) \tag{6}$$

and from $\tilde{\boldsymbol{g}}_h = \mathbf{R}^{-1}\tilde{\boldsymbol{g}}_\mathrm{e}$ it follows that $\tilde{\boldsymbol{g}}_\mathrm{e} = \mathbf{R}\tilde{\boldsymbol{g}}_\mathrm{h}$, which gives

$$\frac{\mathrm{d}\mathbf{R}\tilde{\boldsymbol{g}}_\mathrm{h}}{\mathrm{d}t} = \frac{1}{\tau}(\mathbf{R}\boldsymbol{f}_\mathrm{h} - \mathbf{R}\tilde{\boldsymbol{g}}_\mathrm{h}) \tag{7}$$

Because here $\tilde{\boldsymbol{g}}_\mathrm{e}$ is only an intermediate postulate, we will further use $\tilde{\boldsymbol{g}} = \tilde{\boldsymbol{g}}_\mathrm{h}$. In the last equation $\mathbf{R}$ is still present, but it can be traded in for $\boldsymbol{\omega}$. Appendix C shows the derivation, which then gives

$$\frac{\mathrm{d}\tilde{\boldsymbol{g}}}{\mathrm{d}t} = \frac{1}{\tau}(\boldsymbol{f} - \tilde{\boldsymbol{g}}) - \boldsymbol{\omega} \times \tilde{\boldsymbol{g}} \tag{8}$$

The first term on the right-hand side of (8) gives the estimate of gravity by otolith afferents only. The second term just gives the change of gravity due to rotation only (see also Droulez and Darlot 1989; Viéville and Faugeras 1990; Glasauer 1992a,b). Hence, for low-frequency off-vertical angular motion, $\tilde{\boldsymbol{g}}$ changes according to the output of the otoliths because the canals then do not signal motion, and the low-pass filter passes all information virtually unmodified. For pure blind horizontal (linear) motion, this typically results in a tilt illusion, also referred to as the hilltop illusion[6]. At high frequencies, the otolith output is filtered out almost completely, and $\tilde{\boldsymbol{g}}$ depends predominantly on canal afferents. At intermediate frequencies, as during a head tilt, both systems interact giving a fair estimation of true motion, which is the reason why the time constants of the low-pass filter and the canals should be mutually dependent. Based on SV data obtained in a human centrifuge, de Graaf et al. (1996) reached a value of about 5 s for the low-pass-filter time constant, which is indeed about equal to the main time constant of the canals in humans (Robinson 1977; Raphan et al. 1979; Merfeld et al. 1993). As a result, the rotation matrix $\mathbf{R}$ and its inverse and hence the need to use the elaborate quaternion analysis have been eliminated completely. Instead only a three-component time derivative, a vector or cross product, and two vector subtractions are left.

Furthermore, (8) appears to be the three-dimensional equivalent of the two-dimensional model presented by Mayne (1974), as shown in the intermezzo on Mayne. Also it is equal to the model given by Glasauer (1992a,b), who came to this very same equation based on Kalman–Bucy filter theory (Glasauer 1992a). A slightly, though fundamentally different solution has been presented by Droulez and Darlot (1989), who explicitly take the gravity estimation to be of constant magnitude. Viéville and Faugeras (1990), and Angelaki et al. (1999) thereafter, apply the jerk $\mathrm{d}f/\mathrm{d}t$ to obtain the acceleration of motion using the last term of (8) only. Then, with $\boldsymbol{f} = \tilde{\boldsymbol{a}} + \tilde{\boldsymbol{g}}$ as before, it also follows that

$$\begin{aligned} \frac{\mathrm{d}(\boldsymbol{f} - \tilde{\boldsymbol{a}})}{\mathrm{d}t} = \boldsymbol{\omega} \times (\boldsymbol{f} - \tilde{\boldsymbol{a}}) &\Leftrightarrow \frac{\mathrm{d}\boldsymbol{f}}{\mathrm{d}t} - \frac{\mathrm{d}\tilde{\boldsymbol{a}}}{\mathrm{d}t} = \boldsymbol{\omega} \times \boldsymbol{f} - \boldsymbol{\omega} \times \tilde{\boldsymbol{a}} \\ &\Rightarrow \frac{\mathrm{d}\tilde{\boldsymbol{a}}}{\mathrm{d}t} = \boldsymbol{\omega} \times \tilde{\boldsymbol{a}} + \frac{\mathrm{d}\boldsymbol{f}}{\mathrm{d}t} - \boldsymbol{\omega} \times \boldsymbol{f} \end{aligned} \tag{9}$$

However, by application of (9) alone, the major problem of deficient angular velocity sensors is not solved. Furthermore, as is the case with Droulez and Darlot (1989), Merfeld et al. (1993) and Mergner and Glasauer (1999), some initial value (typically $\boldsymbol{a}_0 = 0$) should explicitly be assumed. These might be acceptable assumptions for robotic purposes (as was the aim of Viéville and Faugeras 1990), but for our CNS such initial settings are implausible postulates as already stated in Sect. 2. Note that according to (8), the initial setting is *not* essential. If, for example $\boldsymbol{g}_0 = 0$ would be set, the sensed gravity vector will finally obtain its proper value, given some knowledge that the system is at rest. This latter fact can be inferred from visual information, but also from the fact that no motor signals are generated to move actively[7]. We therefore conclude that equation (8) gives the most simple and realistic description of how our CNS resolves the GIF-resolution problem.

Intermezzo: Mayne. The two-dimensional model of Mayne (1974) may be redrawn as in Fig. 8, with a translation along the x-axis, $\boldsymbol{g}$ along the z-axis and a rotation about the y-axis. This model is mathematically expressed by

$$\begin{aligned} \frac{\mathrm{d}g_x}{\mathrm{d}t} &= \frac{1}{\tau}(f_x - g_x) - \omega_y \times g_z \\ \frac{\mathrm{d}g_z}{\mathrm{d}t} &= \frac{1}{\tau}(f_z - g_z) + \omega_y \times g_x \end{aligned} \tag{10}$$

which is exactly the two-dimensional portion of (8) with $\omega_x = \omega_z = 0$ (see also Eq. 12). Consequently Mayne predicts the Ferris wheel illusion[8], because if ω is not too large, and the canal afferents have reduced to their resting level (i.e. indicating zero angular velocity), the two gravity components are nonzero and are 90° out-of-phase as is the case with a Ferris wheel gondola.

3.3 Corollaries

As a consequence of (8), it can be shown that if an upright subject is supplied with incongruent information

[6] Equation (8) only predicts the tilt component, while a concomitant vertical component has also been reported. In the latter case the phenomenon is called the hilltop illusion (von Baumgarten et al. 1981), while otherwise the term tiltillusion suffices.

[7] As stated earlier, such inferences are probably *not* realised by genes, but they *can* be made by a neural network using multisensory information.

[8] Which, for dubious reasons, has been denied by Mittelstaedt et al. (1989).

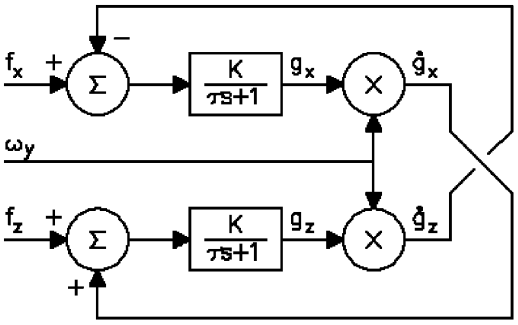

Fig. 8. Block diagram of Mayne's two-dimensional model for resolving the sensed vertical (with its components g_x, and g_z) with f_x, f_z and ω_y as inputs, and with $\dot{g}$ indicating the time derivative of g

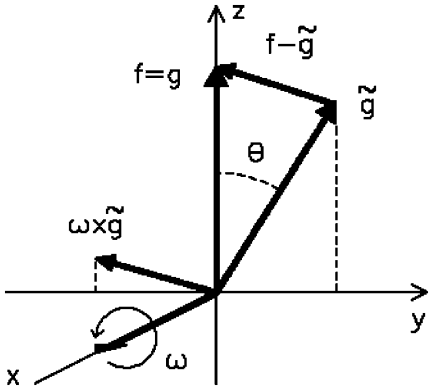

Fig. 9. Rotation of the sensed vertical $\tilde{\boldsymbol{g}}$ by angular velocity $\boldsymbol{\omega}$ (see text)

about rotation around an earth horizontal axis by canal disease or visual stimulation, this will result in a static tilt with respect to true verticality. This is elaborated below.

Intermezzo: Angular velocity induced static tilt. If, due to a canal disease for example, the angular velocity ω is cursed with an offset, this does not necessarily imply a continuous rotation of the sensed vertical. From (8) it can be shown that the sensed vertical only deviates from true verticality by an amount $\theta \approx \omega\tau$. Consider, for example, a supposed rotation about an earth-horizontal axis without a concomitant change of the GIA. Then, $\boldsymbol{f} = \boldsymbol{g}$, and $\boldsymbol{\omega}$ and $\tilde{\boldsymbol{g}}$ are perpendicular (see Fig. 9), the magnitude of $\tilde{\boldsymbol{g}}$ is equal to g, and $|\boldsymbol{\omega} \times \tilde{\boldsymbol{g}}| \approx \omega g$. When ω (and hence θ) is not too large, we have $|\boldsymbol{f} - \tilde{\boldsymbol{g}}| \approx g \sin\theta \approx g\theta$. In that case there is a stable solution to (8) with $\mathrm{d}\tilde{\boldsymbol{g}}/\mathrm{d}t = 0$, and hence since $\tilde{\boldsymbol{g}}$ is constant, this results in

$$\frac{1}{\tau}(\boldsymbol{f} - \tilde{\boldsymbol{g}}) = \boldsymbol{\omega} \times \tilde{\boldsymbol{g}} \Rightarrow \frac{g\theta}{\tau} \approx \omega g \Rightarrow \theta \approx \omega\tau \tag{11}$$

Another condition in which $\boldsymbol{\omega}$ may not be equal to zero, in spite of a static upright position, is that in which a subject is viewing an immersive optic flow field (i.e. without frame or orientational cues), rotating in roll while sitting still. Then, subjects typically experience a dual or ambiguous sensation of a continuous rotation on top of a static tilt. This can also be explained by Fig. 6, in which case we assume that optic flow information is merged with canal output just prior to rotating the earth-fixed frame of reference. The rotation sensation next stems from $\boldsymbol{\omega}_s$, explaining the continuous rotation sensation. Equation (10) then again predicts an additional static tilt. As a result, we therefore predict a simple relationship between the time constant of the vestibular (neuronal) low-pass filter and the angle of the SV($\boldsymbol{g}_s$) relative to true verticality amounting to $\theta \approx \omega\tau$, as induced by a visual phenomenon. This thesis awaits experimental verification.

Another consequence of (8) concerns the canal–otolith interaction with respect to the somatogravic effect in centrifugation. A retardation of the somatogravic effect induced by the angular centrifuge motion can now be understood by considering (8), as described below.

Intermezzo: The somatogravic effect with concomitant angular motion. The tilt of the SV during centrifugation with a fixed arm has been mentioned before. With (8) incorporating angular motion, it can now be better understood. Separation of (8) into its three Cartesian components leads to

$$\begin{aligned}
\frac{\mathrm{d}\tilde{g}_x}{\mathrm{d}t} &= \frac{1}{\tau}(f_x - \tilde{g}_x) - \omega_y\tilde{g}_z + \omega_z\tilde{g}_y \\
\frac{\mathrm{d}\tilde{g}_y}{\mathrm{d}t} &= \frac{1}{\tau}(f_y - \tilde{g}_y) - \omega_z\tilde{g}_x + \omega_x\tilde{g}_z \\
\frac{\mathrm{d}\tilde{g}_z}{\mathrm{d}t} &= \frac{1}{\tau}(f_z - \tilde{g}_z) - \omega_x\tilde{g}_y + \omega_y\tilde{g}_x
\end{aligned} \tag{12}$$

In this equation $\omega_x = \omega_y = 0$ can be substituted and, if the tangential acceleration is ignored, the solution to these coupled differential equations under the boundary condition of $\tilde{g}_x(t=0) = \tilde{g}(t=0) = 0$ yields for the centripetal component:

$$\tilde{g}_{\mathrm{cent}} = \frac{a_{\mathrm{cent}}}{1+\omega^2\tau^2}\left(1 + (\omega\tau\sin\omega t - \cos\omega t)e^{-t/\tau}\right) \tag{13}$$

If a centrifugation is started stepwise, the angular velocity signal generated by the canals according to (A1) reads

$$\omega_{\mathrm{c}} = \omega e^{-t/\tau} \tag{14}$$

and this ω_{c} can next be substituted in to (13). If, for example, $\tau = 10$ s is chosen (arbitrarily) for both the low-pass filter in (13) as well as for the canal decay of ω_{c} in (14), the centripetal component of the sensed vertical can be calculated. Figure 10 shows the effect of the angular motion on the centripetal component of the sensed vertical in this example. Because the resultant angular deviation of the SV with respect to true verticality is given by the inverse tangent of this centripetal component relative to the vertical component, this angle looks roughly like the centripetal component as shown in Fig. 10.

The SV can also be calculated by means of a numerical simulation, so that a more realistic motion onset is realised, and a three-dimensional plot of the sensed vertical can be shown. Two conditions are then of special interest. One is where a subject starts rotating in the centrifuge off centre. Such a result is given in Fig. 11a with an arm length of 5 m and $\omega = 81°/\mathrm{s}$, such that the centripetal acceleration reaches 1 g. In this figure the motion onset is ramped for 2 s, and the sensed vertical is plotted every 0.5 s, starting from the upright position (z-axis aligned). The centre plot (Fig. 11b) shows the effect of shifting out the subject on a sled during 2 s on the centrifuge arm that had already been rotating for two minutes at a constant velocity (same conditions as before). Note that fewer vectors indicate a faster response. In a 5-m fixed and variable arm centrifuge we indeed observed this difference, as is shown in Fig. 12. A similar retardation has been observed by Seidman et al. (1998), who also shifted subjects out on a rotating sled-arm after the canal signal had expired, and found that the delay induced by the dynamic-arm centrifugation was a factor of 4 times smaller than that with fixed-arm centrifugation. Most recently, Merfeld et al. (2001) – in an experiment also using the variable and fixed arm

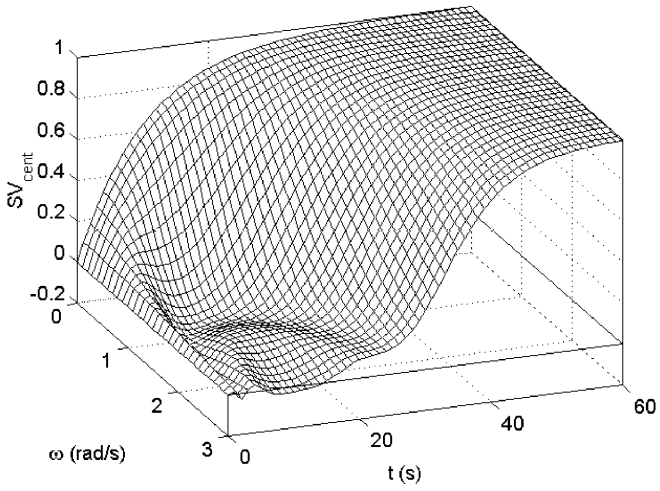

Fig. 10. Somatogravic effect in a centrifuge with a fixed arm. The centripetal component of the sensed vertical is plotted on the vertical axis, with time and centrifuge angular velocity on the base axes (note that at the hypothetical plane $\omega = 0$, an infinitely long arm would be required)

centrifuge paradigms – also observed much faster onset responses in the variable arm conditions, although they did not quantify the difference. These findings all give further support to the description of canal–otolith interaction as presented here. We therefore conclude that time constants of observed tilts in fixed-arm centrifuges do *not only* represent the time constant of the postulated low-pass filter. This also explains an essential part of the wide variation in observed time constants quantifying the somatogravic effect. For example, Guedry (1974) reported values typically larger than 10 s, and Mayne (1974) even took this constant to be 20 s. De Graaf et al. (1996), on the other hand, reported on values of clearly less than 10 s, sometimes even as small as 2 s. All these latter reports concern fixed-arm centrifuge experiments, where different angular velocities have been used.

At relatively high angular velocities, the result on the somatogravic effect merely looks like a pure delay. This is typically observed at additional gravity loads of less than 1 g (see e.g. Fig 12, as well as Seidman et al. 1998). The typical low-pass SV behaviour, as demonstrated for example by Clark and Graybiel (1966), is particularly observed at additional gravity loads of >1 g. Even then, when data of several subjects that only differ in the amount of lag are averaged, their responses will add to a logarithmic curve similar to the output of a low-pass filter. Future research should therefore also focus on individual responses, and averaging over parameters determined in each individual response is preferable to taking the parameters of an averaged response.

In addition to the onset anomalies, Fig. 11c shows a simulated offset response if the subject comes to a stop within 2 s at the end of the centrifuge arm. After constant-velocity rotation, the canals give a false sense of angular velocity just after the deceleration, and these canal afferents rotate the frame of reference such that the SV spirals back to its upright position. The projection of this vertical onto the plane of interest (e.g. the one in which a joy-stick can be manipulated) shows a steep descent, with possibly an undershoot. Such undershoot can indeed be observed (see Fig. 12), and results in a distinct acceleration/deceleration asymmetry in SV behaviour as first observed by Mach (1898). Glasauer (1992c) and Holly (1997), however, do not consider this undershoot during deceleration, which is why Glasauer explicitly adds an inhibiting factor to the rotation term of (8) in his model to cancel the angular velocity when the angle between $\boldsymbol{f}$ and $\boldsymbol{g}$ decreases. Glasauer, however, used a centrifuge with a 10 m long arm, and then only a small angular velocity is required to get the centripetal acceleration (of about 0.6 g), hence reducing the magnitude of the spiralling effect. Moreover, when averaging responses (e.g. as shown by Glasauer, 1992b) individual anomalies such as undershoots with different individual temporal behaviour may be cancelled. This is another reason why future research should focus explicitly on individual responses. Note also that the spiralling effect is two-dimensional, while the responses are recorded in one dimension only, and this – in our personal experience – confounds the results.

A last comment on variable-arm centrifuge experiments is necessary. Additional accelerations have always to be taken into account: the tangential acceleration, the linear acceleration along the sled track itself and the linear Coriolis acceleration perpendicular to the sled motion. Seidman et al. (1998) stated that the canal input may mask the otolith-mediated influence related to tilt, but they ignored the (linear) Coriolis effect, which may be as "overwhelming" as the angular effect itself. This also holds in the case of rotating the subject at the end of a centrifuge arm so as to keep the resultant of the tangential and centripetal acceleration in a head fixed direction (see Cohen et al. 1973). Subjects are then rotated 360° relative to earth within 4 s! As concluded above already, shifting out – all together – is preferable. Linear Coriolis effects will be lower in amplitude and duration than the effects of the angular onset signal using a fixed arm (see Fig. 11). This especially holds for small-arm centrifuges (of less than a few metres radius). To obtain more insight, future SV measurements should thus be performed in at least two planes simultaneously. The sled trick is also preferable in simulating a catapult launch, because it better approaches the catapult launch on an aircraft carrier.

4 Control and observer theory

Low-pass filtering to estimate gravity is only part of the solution for controlling body or eye motion. We will next examine this matter from a control-theoretical point of view. Section 4.1 will explain why we need external models. Section 4.2 will subsequently explain which boundary conditions this internal model should satisfy in order to explain certain spatial-orientation and motion-sickness characteristics.

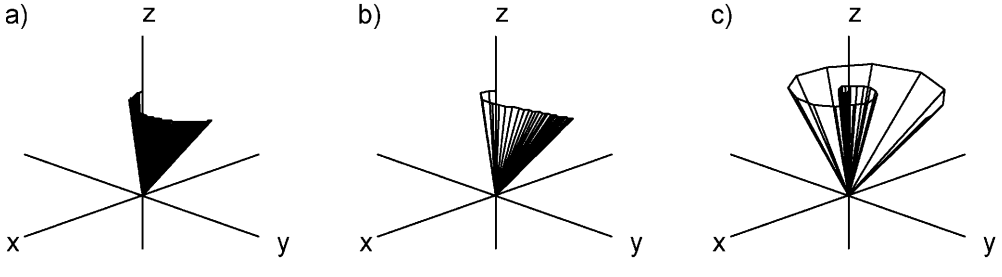

Fig. 11a–c. Sensed vertical plotted every 0.5 s after a centrifuge onset with a fixed arm (**a**) after a shift out on a sled (**b**) and after a centrifuge stop (**c**). See text for further explanation

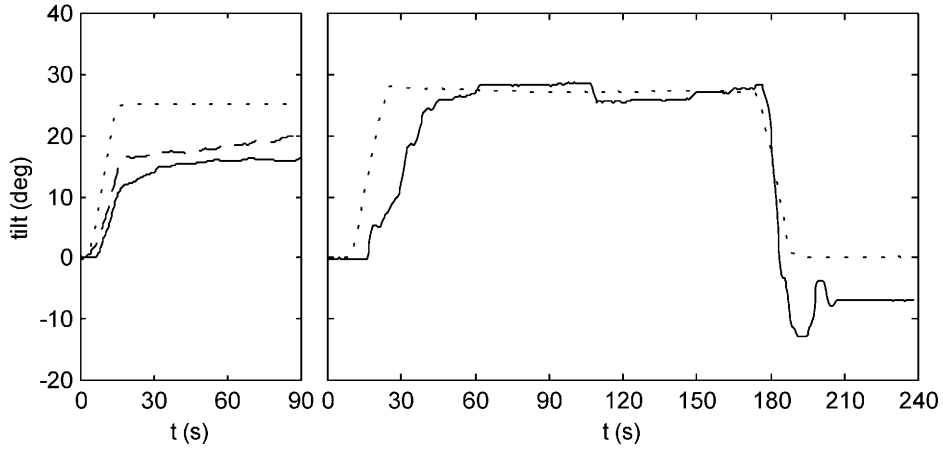

Fig. 12. Observed tilts indicated with a joystick in the dark in a 5-m radius centrifuge rotating at 9.5 rpm resulting in a centripetal lateral acceleration of approximately 0.5 g (*dotted lines* indicate the angle of GIA tilt). Left: Average onset response ($N = 8$) with a fixed arm (*solid line*) and a variable arm (*broken line*). Right: Individual on- and offset response (*solid line*) using a fixed arm. Data taken from de Graaf et al. (1996)

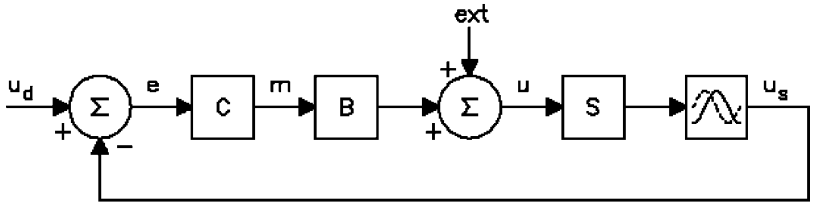

Fig. 13. Simple servomechanism to control body motion, as explained in the text

4.1 Internal models: why

There are at least four variables at stake in controlling body motion: $\boldsymbol{f}, \boldsymbol{a}, \boldsymbol{g}$ and $\boldsymbol{\omega}$, but because two of these are always mutually dependent (i.e. $\boldsymbol{f} = \boldsymbol{a} + \boldsymbol{g}$), only three of them are of real interest. Hence, $\boldsymbol{u} = \boldsymbol{u}(\boldsymbol{a}, \boldsymbol{g}, \boldsymbol{\omega})$ in Fig. 1. A simple servo strategy as discussed below, however, will not work.

> *Intermezzo: Single feedback servo model.* In a simple servo system, a desired body state $\boldsymbol{u}_\mathrm{d}$ (see Fig. 13) is compared with the sensed body state $\boldsymbol{u}_\mathrm{s}$ instead of with a predicted body state $\hat{\boldsymbol{u}}$ as in Fig. 1. To work well, the sensed output ($\boldsymbol{u}_\mathrm{s}$) should then be perfect (i.e. representing the true body state), and delays should be negligible relative to the temporal characteristics of the motions to be controlled. As stated in the previous sections, however, linear acceleration due to motion cannot be assessed perfectly (e.g. the somatogravic effect), nor can angular velocity (e.g. the Ferris wheel illusion). Moreover, the CNS includes neural delays, and the signal $\boldsymbol{u}_\mathrm{s}$ is only available for feedback after many milliseconds. These neural delays may easily lead to instabilities. It is therefore very unlikely that our CNS controls body (or eye) motion by means of such a simple servo strategy. The addition of inverse functions in series with the sensory system in this loop to account for sensor deficiencies will only decrease performance due to the additional delays incurred. Consequently, a different solution should be employed.

The implementation of an internal model as shown in Fig. 1, parallel to the actual (primary) body and sensory systems, may master the shortcomings of a simple servo system. Then again, an error signal $\boldsymbol{e}$ is created, not by using imperfect primary sensory afferents, but by using a predicted body output of $\boldsymbol{u}$ (indicated by $\hat{\boldsymbol{u}}$) instead. This output can be calculated using copies of the transfer functions of the primary path. The benefit of this observer approach is twofold. First, the output $\hat{\boldsymbol{u}}$ lacks the delay of the sensory system, facilitating fast and accurate control of body motion. Second, the imperfections of the sensory apparatus and possibly the CNS function of gravity estimation are duplicated in the internal model. Hence, under optimal performance the output $\hat{\boldsymbol{u}}$ will be equal to $\boldsymbol{u}$ irrespective of any sensor deficiencies and neural delays. A process of habituation will load and subsequently update this internal model, so that impaired function due to disease can be dealt with (vestibular adaptation). The weighting parameters $\mathbf{K}$ used by the internal model to drive the conflict towards zero may include the confidence of the sensed output. Depending on the likelihood or the amount of noise in $\boldsymbol{u}_\mathrm{s}$, this weighting factor should be low (much noise and low accuracy go along with slow tracking) or high (little noise and high accuracy go along with fast tracking). Furthermore, if for whatever reason the difference persists, the CNS may interpret this as a need to update the internal model so as to minimise the conflict.

An early concept of this approach, emphasising the significance of efference copies, was presented by von Holst and Mittelstaedt (1950); see also Mittelstaedt (1975). Oman (1982) presented a model that applied this approach to give the conflict theory on motion sickness a mathematical basis.[9] Optimal estimation theory (i.e. optimising the loop gain $\mathbf{K}$ related to the internal model depending on noise considerations) was applied by Borah et al. (1988), though these authors linearised their model about an upright orientation. Oman's model was adapted by Merfeld et al. (1993) to further explain certain eye-movement characteristics. Although Glasauer

[9] The model of Fig. 1 and Oman's (1982) model are roughly equal. Oman uses a space-state notation, while Fig. 9 merely shows a time-dependent signal flow. Where in Oman's model the internal (weighted-conflict) feedback is returned to the efference copy signal, here the conflict is fed back to the expected body state $\hat{\boldsymbol{u}}$

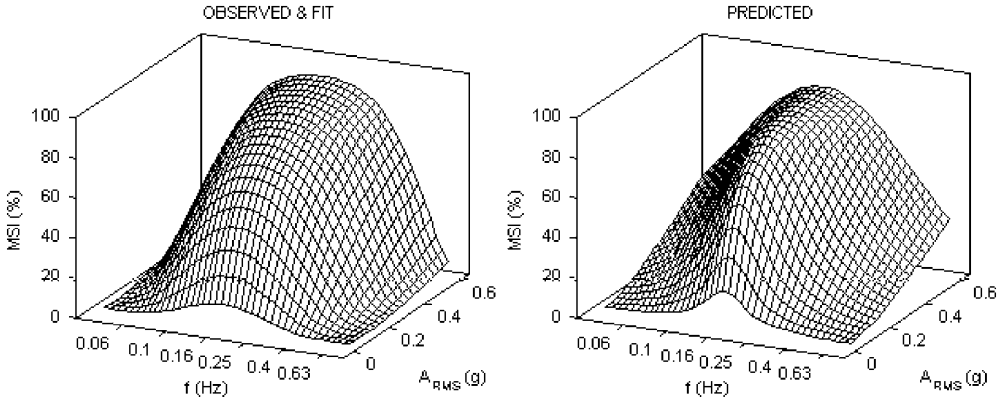

Fig. 14. Motion-sicknes incidence (*MSI*) descriptions. *Left:* Fit through observed MSI-data of over 500 subjects by McCauley et al. (1976) versus frequency (f) and RMS acceleration amplitude (A_{RMS}). *Right:* Predicted data by Bos and Bles (1998). Both curves show an increase of sickness incidence with increasing amplitude, and both also exhibit a peak around 0.16 Hz

and Merfeld (1997) have shown that their models are essentially equal, the relationship with other models remains unclear, and we will elaborate this next.

4.2 Internal models: how

Knowing that we need an internal model for optimal control of body motion is one thing, knowing how to implement it in a model to explain the system's characteristics in real life, such as those of motion sickness, is another. Here we will make an attempt to do so, and some simplifications to the model of Fig. 1 will make this task easier. We may, for example, neglect the effect of action such that the model describes ideal passenger behaviour. The motor signal and its efference copy can then be set to zero, so that $\boldsymbol{u}$ simply represents the external perturbation. Let us furthermore neglect neural delays and angular motions, and assume that (as may be the case for a perfectly tuned system) $\hat{\mathrm{B}} = \mathrm{B}$ and $\hat{\mathrm{S}} = \mathrm{S}$. We will next focus on two ratios, and consider a few simple options. First, $\hat{\boldsymbol{u}}/\boldsymbol{u}$ is of interest, because this ratio should optimally equal 1. Second, $\boldsymbol{c}/\boldsymbol{u}$ is of interest because it represents the relative behaviour of the conflict $\boldsymbol{c}$ regarding motion sickness. Here, one essential characteristic of motion sickness concerns a peak in sickness incidence that occurs at about 0.16 Hz of vertical motion (McCauley et al. 1976; see also Fig. 14 in the example below). The ratio $\boldsymbol{c}/\boldsymbol{u}$ should therefore also show a peak for one typical frequency, i.e. 0.16 Hz. From Fig. 1 it can easily be derived that

$$\frac{\hat{\boldsymbol{u}}}{\boldsymbol{u}} = \frac{\mathrm{K}}{1/\mathrm{S} + \mathrm{K}} \quad \text{and} \quad \frac{\boldsymbol{c}}{\boldsymbol{u}} = \frac{1}{1/\mathrm{S} + \mathrm{K}} \tag{15}$$

and one may consider four basic cases. These cases cover the most simple suppositions possible concerning the transfer functions describing the feedback function K, and the sensor transfer function S:

Case 1: $\mathrm{K} = k$ and $\mathrm{S} = I$ (unit gain). This condition represents a constant feedback gain and perfect sensor characteristics. These choices, however, result in an algebraic loop. Furthermore, if a neural delay were present the system would become instable. Also $\hat{\boldsymbol{u}}/\boldsymbol{u} = k/(1+k)$, and this only gives an optimal solution ($\hat{\boldsymbol{u}} = \boldsymbol{u}$) when $k = \infty$, while stability requires $k < 1$. Note that this solution is used in the literature (e.g. Merfeld et al. 1993; Glasauer and Merfeld 1997). In addition, $\boldsymbol{c}/\boldsymbol{u}$ would then be constant, and this contradicts the observed peak in motion sickness incidence.

Case 2: $\mathrm{K} = k/s$ and $\mathrm{S} = I$. In this case the feedback gain is increasing over time, hence indicating some "learning" capacity. Here, $\hat{\boldsymbol{u}}/\boldsymbol{u} = (k/s)/(1 + k/s) = \tau/(\tau s + 1)$ with $\tau = 1/k$, which implicitly gives the internal model a low-pass filter characteristic, and $\hat{\boldsymbol{u}}$ could represent gravity. However, $\boldsymbol{c}/\boldsymbol{u} = 1/(1 + k/s) = \tau s/(\tau s + 1)$, which represents a high-pass filter, and this contradicts the observed data too.

Case 3: $\mathrm{K} = k$ and $\mathrm{S} = 1/(\tau s + 1)$. Here, it is supposed that the sensor (i.e. otolith) afferents are low-pass filtered explicitly both in the sensor path as well as in the internal model. Then $\hat{\boldsymbol{u}}/\boldsymbol{u} = k/(\tau s + 1 + k)$, and this again equals a low-pass function. Now, $\boldsymbol{c}/\boldsymbol{u} = 1/(\tau s + 1 + k)$, and this also represents a low-pass filter, whose output is again contradictory to the observed data.

Case 4: $\mathrm{K} = k/s$ and $\mathrm{S} = 1/(\tau s + 1)$. Here $\hat{\boldsymbol{u}}/\boldsymbol{u} = k/(\tau s^2 + s + k)$, and this once more represents a low-pass filter function. In this case $\boldsymbol{c}/\boldsymbol{u} = s/(\tau s^2 + s + k)$, which represents a band-pass filter with a characteristic as observed.

These considerations lead to the conclusion that K should include an integration. Moreover, if neural delays were present, then by substituting a pure temporal delay (e.g. $\mathrm{S} = e^{-\tau s}$), the system would even become instable if K were only a gain. This is yet another reason speaking in favour of $\mathrm{K} = k/s$. We furthermore conclude that S should include a low-pass filter, and hence the model of Fig. 1 should explicitly incorporate two gravity estimators, instead of having the internal model function as a gravity estimator implicitly. Only then can the observed frequency peak in motion sickness incidence be explained. Below we will further elaborate this example. If angular motion is not neglected, and all six degrees of freedom are at stake, S should consequently be substituted by equation (8).

Intermezzo: Motion sickness. Oman (1982) originally presented his model to give the conflict theory on motion sickness a mathematical basis. This theory by Reason and Brand (1975) states that: ''Motion sickness occurs at the onset and cessation of conditions of sensory rearrangement when the pattern of inputs from the vestibular system, other proprioceptors and vision is at variance with the stored patterns derived from recent transactions with the spatial environment''. This ''variance'' is nicely explained by the conflict $\boldsymbol{c}$ shown in Fig. 1. Oman, however, did not present quantitative data.

Furthermore, this model does not describe motion sickness characteristics as they are observed, because no explicit low-pass filter was applied in both afferent paths as explained above. Bles (1998), Bles et al. (1998) and Bos and Bles (1998) adapted this model as follows. We first noted that people only get sick if: (a) they do have a functioning vestibular apparatus, (b) gravity changes relative to their body/head and (c) they anticipate this gravity component incorrectly. The first fact necessitates the explicit use of vestibular afferents in the model. The second fact was put forward because purely on-axis rotations around an earth-vertical axis are hardly provocative, whereas the same rotation about an earth-horizontal axis is extremely provocative. Moreover, Bles and de Graaf (1993) also reported subjects making head movements *after* a 1 h 3G centrifuge run. These persons got sick when making rolling and pitching head movements when upright, and when making rolling and yawing head movements when supine. Head rotations about the earth-vertical were clearly the least provocative in all conditions. The third fact concerning anticipation was the primary rationale for postulating an internal model to explain motion sickness. We hence concluded that only the $\Delta\boldsymbol{g}$ component in $\boldsymbol{c}$ (remember $\boldsymbol{u} = \boldsymbol{u}(\boldsymbol{a}, \boldsymbol{g}, \boldsymbol{\omega})$) correlates with motion sickness, and accordingly implemented two explicit low-pass filters in both sensor and internal model paths to be able to obtain this difference (Bos and Bles 1998). We next applied these insights to a passenger model, with an integrator in the internal model feedback path ($\mathrm{K} = k/s$). Because the gravity conflict can become large – both negative and positive – whereas motion sickness only ranges from not sick (0% sickness) to vomiting at its extreme (100% sickness), a Hill-type function is used to transform the conflict conform this asymptotic behaviour:

$$\mathrm{H} = \frac{c^2}{b^2 + c^2} \tag{16}$$

where H is taken from Fig 1, and $c^2 = \boldsymbol{c} \cdot \boldsymbol{c}$ using the dot product. As it is observed that sickness only increases gradually within a period of several minutes up to two hours after motion onset (McCauley et al. 1976), an additional leaky integrator is finally applied to the output of the Hill function to account for these cumulative effects (Oman 1982). Due to the long time constant of this filter ($\mu = 12$ min typically, cf. Bos and Bles, 1998), this integrator averages out short temporal fluctuations and only affects the final output amplitude, independent of input frequencies[10]. Then the output can be calculated using, for example, a sinusoidal vertical motion such as those used by McCauley et al. (1976). Figure 14 shows both the original description of McCauley et al. (based on observed data) and our model predictions. Here, the output is represented as the percentage of a population reaching the limit of vomiting (called the motion-sickness incidence), within two hours of endured motion. Note that a peak is indeed predicted as observed, whose location only depends on the time constant τ as fixed by the somatogravic effect and the internal model feedback gain k (here $\tau = 5$ s and $k = 1$ s^{-1}). The appearance of the curvature (flatness) is further determined by factor b of the Hill function. Although there are many assumptions in the model (e.g. ideal passenger), the fact that the two models look very similar is rewarding.

Furthermore, also in this example, the time constant of the low-pass filter is required to be much smaller than that observed in the somatogravic effect using a centrifuge as described above. Taking a larger time constant would shift the peak in sickness incidence far above 0.2 Hz, which is contradictory to the observations by McCauley et al. and this also speaks in favour of a time constant in the order of seconds, instead of tens of seconds.

[10] Because of this long time constant, it is not a realistic option to take a leaky integrator in the post-conflict processing in combination with $\mathrm{K} = k/s$ and $\mathrm{S} = I$ (Case 2 in Sect. 4.2). Then, the total transfer function also acts as a band limiting filter (e.g. when neglecting the Hill function for the moment, $\boldsymbol{c}/\boldsymbol{u} = \tau s/(\tau s + 1) * 1/(\mu s + 1)$. The high-pass cut-off frequency would then be far below 0.01 Hz, and this is not observed (see McCauley et al. 1976).

4.3 Corollaries

Here it is interesting to speculate about the interaction of somatogravic and visual signals. First, only people without a functioning vestibular apparatus are insensitive to motion sickness. Thus the somatosensory and vestibular signals should be treated differently at an early stage in the model (see Fig. 6). Second, if we base our sense of $\boldsymbol{a}, \boldsymbol{g}$, and $\boldsymbol{\omega}$ on integrated information from all our senses, we may well assume that this single integrated signal is also effective as the only input for all subsystems in the internal model. An additional input to the internal model originates from our cognitive system. For example, if a joystick would be spring-loaded, such as to reset the stick in an upright position when released (e.g. Seidman et al. 1998), this null setting will act as an attractor. It can contribute to the cognitive inference about the true orientation of gravity, even if the joystick only supplies egocentric information and the subject knows that the centrifuge chair cannot be tilted.

It is a fundamental property of the controller C in Fig. 1 that it only generates signals representing motion (i.e. $\boldsymbol{a}$ and $\boldsymbol{\omega}$, and *not* attitude (i.e. $\boldsymbol{g}$). Concerning the angular velocity feedback, Droulez and Darlot (1989) and Merfeld et al. (1993) have shown that by means of an internal model (be it without an additional efference copy), velocity storage (Raphan et al. 1979) can be predicted successfully. Then the weighted angular velocity feedback results in a nystagmus decay that is slower than that predicted by canal function only (Eq. A1). Note that in this description, the GIF resolution is not at stake. If it is, the role of gravity has been smuggled. Attitude is only controlled indirectly by the other two variables $\boldsymbol{a}$ and $\boldsymbol{\omega}$. Consequently, there can also be no efference copy representing gravity, and the internal model therefore lacks this component. When including a copy of otolith function in the internal model, an expected GIA (or $\hat{\boldsymbol{f}}$) should be an input to this function, and the gravity estimator $\tilde{\boldsymbol{g}}$ or an additional feedback signal coming from $\hat{\boldsymbol{g}}_{\mathrm{s}} - \tilde{\boldsymbol{g}}_{\mathrm{s}}$ can be used for this purpose. In the example on motion sickness we have successfully applied the latter. This, however, remains a disputable solution, because it necessitates an additional feedback loop without a matching efference copy, while

$\tilde{\boldsymbol{g}}$ is a simple alternative without the need of an additional feedback loop. A solution to this problem is not directly at hand.

A solution may be obtained indirectly by means of periodical otolith stimulation, as used by Glasauer (1992a,b, 1995), and Seidman et al. (1998). Glasauer, specifically, observed SV gains as predicted by the Mayne equation, whereas the observed phase lags were much smaller. To account for this he applied a simple phase correction in his model (Glasauer, 1992a), but Glasauer (1995) states that probably a predictive mechanism must be at work. If the SV is driven directly by the gravity output of the internal model ($\hat{\boldsymbol{g}}$), the results of such experiments may favour one of the solutions as mentioned above.

It may be argued that if no appropriate efference copy is involved at all, as in the case with passive motion (i.e. a passenger on a ship), an internal model is rudimentary. This indeed may be the case. Humans and animals naturally move themselves actively, and efference copies are of value. Apparently this system still functions when we move passively, although not serving any function then, and its effect may even be negative (i.e. we get sick). Whilst sleeping, we normally do not move actively in the sense of locomotion and the internal model may well be switched off! This seems to be true, because people do *not* get sick when asleep (there are no reports on the contrary). Moreover, for mechanical reasons slugs move much slower and have less problems with posture than bipeds, and plants do not move at all so they also do not need to know their motion, and apparently these species do not show any signs or symptoms of motion sickness.

One concern with eye movements relates to the unresolved question as to whether eye movements and subjective or cognitively biased responses, such as a verbal or manually indicated estimates of angular velocity, do always correlate. For example, Okada et al. (1999) observed that the decay of perceived angular velocity is approximately equal to that of the nystagmus decay when rotating about an earth vertical axis in *yaw*. This nystagmus decay is prolonged by velocity storage (Raphan et al. 1979), and it may therefore be assumed that the perceived angular velocity decay is also prolonged by velocity storage. However, when rotating in *roll*, there is no velocity storage involved (e.g. Bos et al. 2002; Tweed et al. 2001; Bos et al. 1994a,b), but in this case a correlation between the perceived and eye movement angular velocity has not been studied yet.

Another concern with eye movements relates to the compensation for deficient canal information by using additional otolith information as applied by Merfeld et al. (1993, 1999), Glasauer and Merfeld (1997) and, in a rudimentary form, also by Crane and Demer (1999). Mergner and Glasauer (1999) have used additional otolith information to also estimate angular motion, to try to solve the GIF-resolution problem. Using otolith afferents makes sense because the Cartesian vector components of gravity do change during rotations about an off-vertical axis. To this end a vector product of the true otolith output and that of the internal model can be used. By doing so the aforementioned authors implicitly create an error signal with the same dimension as angular velocity. An explicit explanation is given in appendix D of this paper. This error signal has been given much weight in the Merfeld et al. model when explaining observed eye movements. Then, however, the subjective rotations may also depend on this otolith angular velocity. Their model would therefore also predict a persistent sense of rotation during an off-vertical axis rotation. This contradicts the Ferris wheel illusion, and either eye movements are essentially different from other subjective responses, or the concept of otolith angular velocity is wrong. This topic also needs further elaboration.

5 Conclusion

5.1 Canal–otolith interaction

Here we have shown that several models describing the GIF resolution problem are in fact equal (Mayne 1974; Glasauer 1992a,b; Bles and de Graaf 1993; and partly Viéville and Faugeras, 1990), and are given by one canal–otolith interaction differential equation (8). Essential in these descriptions is the fact that gravity is resolved from otolith afferents by low-pass filtering after rotating the frame of reference to an earth-fixed frame using canal afferents. These models therefore all correctly predict both the somatogravic effect and the Ferris wheel illusion. We also showed that perceived motion behaves like the counterpart of perceived tilt, i.e. like a high-pass derivative of otolith afferents. In these models *no* initial settings are required, assuming that additional information is available on conditions of being at rest. As a consequence we explained part of the large variability in observed time constants of the somatogravic effect by concomitant angular centrifuge motion. Furthermore, from tilt and translation data from centrifugation and horizontal oscillation, as well as from motion sickness data, we conclude that the time constant of the low-pass filter is in the order of seconds instead of tens of seconds as previously assumed. Because (8) plays such a vital role in the vestibular part of spatial orientation, and Mayne (1974) first described it (albeit in two dimensions instead of three), it might as well be called the Mayne equation.

5.2 Internal model

Other models that also use a canal rotation, but without an explicit low-pass filter function, have also been presented (Oman 1982; Droulez and Darlot 1989; Viéville and Faugeras 1990; Merfeld et al. 1993, 1999; Angelaki et al. 1999; Mergner and Glasauer 1999). Of these, Oman, Droulez and Darlot, and Merfeld et al. have used an internal model, Oman to explain (but not to quantify) motion sickness, and the others to explain and quantify certain eye-movement characteristics. However, the relationship with the GIF-resolution,

and successful quantitative predictions have not been shown previously. Here we have shown that we indeed need internal models for control purposes, and that an internal model may act implicitly as a low-pass filter to solve the GIF problem.

5.3 Integration

One of the main issues in the present paper is how by means of observer theory, where sensor afferents *and* internal model afferents are both explicitly filtered to obtain estimates of gravity, a frequency-dependent peak in motion sickness severity is predicted as observed. The location of this frequency peak is determined by the time constant of the low-pass filter as inferred from the somatogravic effect. It therefore seems likely that our CNS not only applies an internal model for the control of certain motions (cf. Merfeld et al. 1999), but it applies the basic canal–otolith interaction description twice in addition. In fact, this explicit implementation of the Mayne equation operating both on the sensor afferents as well as in the internal model reflects the coherence constraint introduced by Droulez and Darlot (1989).

Acknowledgements. We would like to thank our colleagues R. Hosman and P. Wewerinke from TNO, and B.L.G. Bakker and T.J.C. Faes from the Vrije Universiteit, Amsterdam, for their help and fruitful discussions on this topic, as well as the reviewers, especially the one who gave very extensive and useful comments. The data of Figs. 5 and 12 were gathered together with Dr. de Graaf from TNO at the Coriolis Acceleration Platform of the Naval and Aerospace Medical Research Laboratory in Pensacola, Florida, for which we are also obliged to Drs. A. Rupert and F. Guedry. Mr. D. Cable turned our text into English. The Royal Netherlands Air Force and the Royal Netherlands Navy funded the work that contributed to this paper.

Appendix A: Elementary facts

Throughout this paper, scalars (quantities denoted by a single number) are given in italics, and vectors (quantities denoted by a series of numbers) in italics and bold type. Matrices (operators to convert a vector into another, like a rotation) are given by capital letters in bold types, and quaternions (see Appendix B) are in bold type. Where appropriate, $\boldsymbol{\theta}$ and $\boldsymbol{\omega}$ represent angular position and velocity, and $\boldsymbol{a}$ (and $\boldsymbol{f}$ and $\boldsymbol{g}$) linear acceleration. Furthermore, it is important to note that the length of a vector does not change by rotation, which can also be considered a consequence of the orthogonality principle. That is, the elements r_{ij} of a rotation matrix $\mathbf{R}$ satisfy $\Sigma r_{ij} r_{ik} = \delta_{jk}$, where $\delta_{jk} = 1$ if $j = k$, and 0 otherwise. The matrix $\mathbf{R}$ is called orthogonal. This implies that the inverse rotation can be given by its transposed (or mirror image): $\mathbf{R}^{-1} = \mathbf{R}^{\mathrm{T}}$. If $\mathbf{R}(\theta)$ represents a rotation around some axis by the angle θ, $\mathbf{R}^{-1}(\theta) = \mathbf{R}(-\theta)$.

When dealing with body displacements, acceleration is preferable over force to work with, because it does not depend on body mass. Furthermore, we sense gravity by its reaction force, so that in this context the gravitational acceleration is directed out of the earth (gravity pulls the otoconia in the otoliths down, which matches a translational acceleration upward). The resultant linear acceleration $\boldsymbol{f}$ due to motion $\boldsymbol{a}$ and gravity $\boldsymbol{g}$, is also called the GIA. 1 g refers to an acceleration equal to the earth gravitational acceleration (1 g $\approx$ 9.81 m/s^2), while 1 G refers to the force exerted by a 1 g acceleration.

Within the vestibular system the GIA is sensed by the otolithic system, whereas angular motions are registered by the SCC, both in a head-fixed coordinate frame. Despite the complex anatomical organisation of the otoliths (Lindeman 1973) and its neuronal responses (Fernandez and Goldberg, 1976a–c), the otolith transfer function can be approximated by an identity, which suits the present purpose in the range of natural frequencies, that is, below 5 Hz (see also Merfeld et al. 1993). The canals, however, mainly function as angular velocity sensors, albeit only for varying velocities within in the range of about 0.05 to 5 Hz (Steinhausen 1931, 1933; Lowenstein and Sand 1940; van Egmond et al. 1949; Groen 1956, 1957; Mayne 1974; Howard 1986; Muller 1990). A function that most simply describes such behaviour is that of a high-pass filter. Then, for varying velocities the output corresponds to the velocity, and for sustained constant input velocities the output is zero. Hence the canal transfer function can be approximated by (see also Robinson 1977; Raphan et al. 1979; Merfeld et al. 1993)

$$\frac{\omega_{\mathrm{scc}}}{\omega_{\mathrm{in}}} = \frac{\tau s}{\tau s + 1} \tag{A1}$$

Appendix B: Rotation matrix related to angular velocity using quaternions

Suppose two coordinate frames, one rotated with an angular velocity $\boldsymbol{\omega}$ with respect to the other. Let $\boldsymbol{x}$ be an arbitrary vector, and $\boldsymbol{y}$ its representation with respect to the rotated frame

$$\boldsymbol{y} = \mathbf{R}\boldsymbol{x} \quad \text{or} \quad \boldsymbol{x} = \mathbf{R}^{-1}\boldsymbol{y} \quad \text{with} \quad \mathbf{R} = \begin{pmatrix} r_{11} & r_{12} & r_{13} \\ r_{21} & r_{22} & r_{23} \\ r_{31} & r_{32} & r_{33} \end{pmatrix} \tag{B1}$$

The basic equation that relates the elements of $\mathbf{R}$ to $\boldsymbol{\omega}$ is given by Tweed and Vilis (1987):

$$\frac{\boldsymbol{\omega}}{2}\mathbf{r} = \frac{\mathrm{d}\mathbf{r}}{\mathrm{d}t} \tag{B2}$$

where $\boldsymbol{\omega}$ and $\mathbf{r}$ represent quaternions (see Altmann 1986), with a scalar and a vector part:

$$\boldsymbol{\omega} = 0 + \boldsymbol{\omega} = 0 + \omega_x\hat{x} + \omega_y\hat{y} + \omega_z\hat{z} \tag{B3}$$

and

$$\mathbf{r} = r_0 + \boldsymbol{r} = r_0 + r_x\hat{\boldsymbol{x}} + r_y\hat{\boldsymbol{y}} + r_z\hat{\boldsymbol{z}} = |r|(D + A\hat{\boldsymbol{x}} + B\hat{\boldsymbol{y}} + C\hat{\boldsymbol{z}}) \tag{B4}$$

with

$$|\mathbf{r}| = \sqrt{r_0^2 + r_x^2 + r_y^2 + r_z^2} \tag{B5}$$

From this, it can be inferred that

$$\begin{aligned} &D = \cos\theta, \quad A = \sin\theta\cos\alpha, \quad B = \sin\theta\cos\beta, \\ &C = \sin\theta\cos\gamma \end{aligned} \tag{B6}$$

which defines $\mathbf{R}$ as a rotation about $\boldsymbol{\omega}$ by an angle 2θ (with α, β and γ representing the angles between the rotation axis and the x, y, and z coordinate-frame axes respectively). In (B2), the product of two quaternions r and s is used, which satisfies

$$\mathbf{rs} = r_0 s_0 - \boldsymbol{r}\cdot\boldsymbol{s} + r_0\boldsymbol{s} + s_0\boldsymbol{r} + \boldsymbol{r}\times\boldsymbol{s} \tag{B7}$$

and

$$\frac{\mathrm{d}\mathbf{r}}{\mathrm{d}t} = \frac{\mathrm{d}r_0}{\mathrm{d}t} + \frac{\mathrm{d}r_x}{\mathrm{d}t}\hat{\boldsymbol{x}} + \frac{\mathrm{d}r_y}{\mathrm{d}t}\hat{\boldsymbol{y}} + \frac{\mathrm{d}r_z}{\mathrm{d}t}\hat{\boldsymbol{z}} \tag{B8}$$

This all combines into

$$\frac{\boldsymbol{\omega}}{2}\mathbf{r} = \tfrac{1}{2}(-\boldsymbol{\omega}\cdot\boldsymbol{r} + r_0\boldsymbol{\omega} + \boldsymbol{\omega}\times\boldsymbol{r}) = \frac{\mathrm{d}\mathbf{r}}{\mathrm{d}t} \tag{B9}$$

From (B9), r_0, r_x, r_y and r_z can be obtained, and either by (B4) and (B5), or by (B6) A, B, C and D can be found. The elements r_{ij} from $\mathbf{R}$ as given in (B1) are finally given by Westheimer (1957):

$$\begin{aligned} r_{11} &= D^2 + A^2 - B^2 - C^2 \\ r_{21} &= 2(AB - CD) \\ r_{31} &= 2(AC + BD) \\ r_{12} &= 2(AB + CD) \\ r_{22} &= D^2 - A^2 + B^2 - C^2 \\ r_{32} &= 2(BC - AD) \\ r_{13} &= 2(AC - BD) \\ r_{23} &= 2(BC + AD) \\ r_{33} &= D^2 - A^2 - B^2 + C^2 \end{aligned} \tag{B10}$$

Appendix C: Kinematic derivation of the general SV-differential equation

The differential equation describing the subjective vertical SV ($\tilde{\boldsymbol{g}}$) by means of the rotation matrix $\mathbf{R}$ according to (5) is

$$\frac{\mathrm{d}\mathbf{R}\tilde{\boldsymbol{g}}}{\mathrm{d}t} = \frac{1}{\tau}(\mathbf{R}\boldsymbol{f} - \mathbf{R}\tilde{\boldsymbol{g}}) \tag{C1}$$

Applying the product rule for differentiation to the left-hand side of this equation, we get

$$\frac{\mathrm{d}\mathbf{R}}{\mathrm{d}t}\tilde{\boldsymbol{g}} + \mathbf{R}\frac{\mathrm{d}\tilde{\boldsymbol{g}}}{\mathrm{d}t} = \frac{1}{\tau}(\mathbf{R}\boldsymbol{f} - \mathbf{R}\tilde{\boldsymbol{g}}) \tag{C2}$$

Application of $\mathbf{R}^{-1}$ to both sides results in

$$\frac{\mathrm{d}\tilde{\boldsymbol{g}}}{\mathrm{d}t} = \frac{1}{\tau}(\boldsymbol{f} - \tilde{\boldsymbol{g}}) - \mathbf{R}^{-1}\frac{\mathrm{d}\mathbf{R}}{\mathrm{d}t}\tilde{\boldsymbol{g}} \tag{C3}$$

If we now focus on what happens to a vector $\boldsymbol{x}$ if it is only rotated, and call $\boldsymbol{y} = \mathbf{R}\boldsymbol{x}$, we have

$$\frac{\mathrm{d}\boldsymbol{y}}{\mathrm{d}t} = \frac{\mathrm{d}\mathbf{R}}{\mathrm{d}t}\boldsymbol{x} \quad \text{and} \quad \frac{\mathrm{d}\boldsymbol{y}}{\mathrm{d}t} = \boldsymbol{\omega}\times\boldsymbol{y} \tag{C4}$$

where $\boldsymbol{\omega}$ is given in the same frame as $\boldsymbol{y}$. In combination this becomes

$$\frac{\mathrm{d}\mathbf{R}}{\mathrm{d}t}\boldsymbol{x} = \boldsymbol{\omega}\times\boldsymbol{y} \tag{C5}$$

Because $\boldsymbol{x}$ could be any vector, e.g. $\tilde{\boldsymbol{g}}$ as well as $\boldsymbol{\omega}$, we thus have

$$\frac{\mathrm{d}\mathbf{R}}{\mathrm{d}t}\tilde{\boldsymbol{g}} = \mathbf{R}\boldsymbol{\omega}\times\mathbf{R}\tilde{\boldsymbol{g}} \tag{C6}$$

Because $\mathbf{R}\boldsymbol{x}\times\mathbf{R}\boldsymbol{y} = \mathbf{R}(\boldsymbol{x}\times\boldsymbol{y})$ for rotations, application of $\mathbf{R}^{-1}$ to both sides of the latter result finally gives a mathematical equivalent of (C1)

$$\frac{\mathrm{d}\tilde{\boldsymbol{g}}}{\mathrm{d}t} = \frac{1}{\tau}(\boldsymbol{f} - \tilde{\boldsymbol{g}}) - \boldsymbol{\omega}\times\tilde{\boldsymbol{g}} \tag{C7}$$

Appendix D: Angular velocity from otolith afferents

Suppose, as before, that $\boldsymbol{f}$ represents the otolith output, and $\hat{\boldsymbol{f}}$ the otolith output in the internal model. Then, if $\boldsymbol{f}$ and $\hat{\boldsymbol{f}}$ would only differ by rotation, and we treat the difference $\boldsymbol{f} - \hat{\boldsymbol{f}}$ as a time derivative[1]

$$\boldsymbol{f} - \hat{\boldsymbol{f}} \propto \boldsymbol{f}(t) - \boldsymbol{f}(t - \Delta t) \propto \mathrm{d}\boldsymbol{f}/\mathrm{d}t. \tag{D1}$$

for which $\mathrm{d}\boldsymbol{f}/\mathrm{d}t = \boldsymbol{\omega}\times\boldsymbol{f}$, we have

$$\boldsymbol{f} - \hat{\boldsymbol{f}} \propto \boldsymbol{\omega}\times\boldsymbol{f} \tag{D2}$$

By applying the vector product with $\boldsymbol{f}$ to both sides we get

$$\begin{aligned} &\boldsymbol{f}\times\left(\boldsymbol{f} - \hat{\boldsymbol{f}}\right) \propto \boldsymbol{f}\times\boldsymbol{\omega}\times\boldsymbol{f} \\ &\quad \Rightarrow \boldsymbol{f}\times\boldsymbol{f} - \boldsymbol{f}\times\hat{\boldsymbol{f}} \propto \boldsymbol{\omega}(\boldsymbol{f}\cdot\boldsymbol{f}) - \boldsymbol{f}(\boldsymbol{f}\cdot\boldsymbol{\omega}) \end{aligned} \tag{D3}$$

Because $\boldsymbol{f}\times\boldsymbol{f} = 0$, and $\boldsymbol{\omega}$ is always perpendicular to the plane in which $\boldsymbol{f}$ changes such that $\boldsymbol{f}\cdot\boldsymbol{\omega} = 0$, this reduces to

$$-\boldsymbol{f}\times\hat{\boldsymbol{f}} \propto f^2\ \boldsymbol{\omega} \Rightarrow \boldsymbol{\omega} \propto \frac{\hat{\boldsymbol{f}}\times\boldsymbol{f}}{f^2} \tag{D4}$$

[1] It may also be argued that due to neural delays, $\hat{\boldsymbol{f}}$ will always lag $\boldsymbol{f}$ by some amount Δt.

References

Altmann SL (1986) Rotations, quaternions and double groups. Clarendon, Oxford

Angelaki DE, Hess BJM (1996a) Three-dimensional organization of otolith-ocular reflexes in rhesus monkeys. I. Linear acceleration responses during offvertical axis rotation. J Neurophysiol 75: 2405–2424

Angelaki DE, Hess BJM (1996b) Three-dimensional organization of otolithocular reflexes in rhesus monkeys. II. Inertial detection of angular velocity. J Neurophysiol 75: 2425–2440

Angelaki DE, McHenry MQ, Dickman JD, Newlands SD, Hess BJM (1999) Computation of inertial motion: neural strategies to resolve ambiguous otolith information. J Neurosci 19: 316–327

Baumgarten RJ von, Vogel H, Kass JR (1981) Nauseogenic properties of various dynamic and static force environments. Acta Astronaut 8: 1005–1013

Bles W (1998) Coriolis effects and motion sickness modelling. Brain Res Bull 47: 543–549

Bles W, Graaf B de (1993) Postural consequences of long duration centrifugation. J Vestib Res. 3: 87–95

Bles W, Bos JE, Graaf B de, Groen E, Wertheim AH (1998) Motion sickness: Only one provocative conflict? Brain Res Bull 47: 481–487

Bles W, Bos JE, Kruit H (2000) Motion sickness. Curr Opin Neurol 13: 19–25

Borah J, Young LR, Curry RE (1988) Optimal estimator model for human spatial orientation. Ann N Y Acad Sci 545: 51–73

Bos JE, Bles W (1998) Modelling motion sickness and subjective vertical mismatch detailed for vertical motions. Brain Res Bull 47: 537–542

Bos JE, Bles W, de Graaf B (2002) Eye movements to yaw, pitch, and roll about vertical and horizontal exes, adaptation, and motion sickness. Aviat Space Environ Med, in press

Bourdon B (1906) Influence de la force centrifuge sur la perception de la verticale. Ann Psychol 12: 8494

Clark B, Graybiel A (1949) Apparent rotation of a fixed target associated with linear acceleration in flight. Am J Ophthalmol 32: 549–557

Clark B, Graybiel A (1963) Contributing factors in the perception of the oculogravic illusion. Am J Psychol 76: 18–27

Clark B, Graybiel A (1966) Factors contributing to the delay in the perception of the oculogravic illusion. Am J Psychol 79: 377–388

Cohen MM, Crosbie RJ, Blackburn LH (1973) Disorienting effects of aircraft catapult launches. Aerosp Med 44: 37–39

Crane BT, Demer JL (1999) A linear canal-otolith interaction model to describe the human vestibulo-ocular reflex. Biol Cybern 81: 109–118

Droulez J, Darlot C (1989) The geometric and dynamic implications of the coherence constraints in three-dimensional sensorimotor interactions. In: Jeannerod M (ed) Attention and performance. Erlbaum, Mahwah, N.J., pp 495–562

Egmond AAJ van, Groen JJ, Jongkees LBW (1949) The mechanics of the semicircular canal. J Physiol (Lond) 110: 1–17

Fernandez C, Goldberg JM (1976a) Physiology of peripheral neurons innervating otolith organs of the squirrel monkey. I. Response to static tilts and to longduration centrifugal force. J Neurophysiol 39: 970–984

Fernandez C, Goldberg JM (1976b) Physiology of peripheral neurons innervating otolith organs of the squirrel monkey. II Directional selectivity and forceresponse relations. J Neurophysiol 39: 985–995

Fernandez C, Goldberg JM (1976c) Physiology of peripheral neurons innervating otolith organs of the squirrel monkey. III Response dynamics. J Neurophysiol 39: 996–1008

Gibson JJ (1952) The relation between visual and postural determinants of the phenominal vertical. Psychol Rev 59: 370–375

Gibson JJ, Mowrer OH (1938) Determinants of the perceived vertical and horizontal. Psychol Rev 45: 300–323

Glasauer S (1992a) Das Zusammenspiel von Otolithen und Bogengangen im Wirkungsgefuge der subjektiven Vertikale (in German). Thesis, Technische Universität München, Munich, Germany

Glasauer S (1992b) Interaction of semicircular canals and otoliths in the processing structure of the subjective zenith. Annals of the New York Academy of Sciences 656: 847–849

Glasauer S (1992c) Human spatial orientation during centrifuge experiments: Nonlinear interaction of semicircular canals and otoliths. In: Proceedings of the 17th Proc. Barany Society. Meeting, Prague, Czechoslovakia, Krejcova H, Jerabek J(eds) 48–52

Glasauer S (1995) Linear acceleration perception: frequency dependence of the hilltop illusion. Acta Otolaryngol Suppl 520: 37–40

Glasauer S, Merfeld DM (1997) Modelling threedimensional vestibular responses during complex motion stimulation. In: Fetter M, Haslwanter T, Misslisch H, Tweed D (eds) Threedimensional kinematics of eye, head and limb movements. Harwood, Amsterdam; pp 387–398

Graaf B de, Bos JE, Tielemans W, Rameckers F, Rupert AH, Guedry FE (1996) Otolith contribution to ocular torsion and spatial orientation during acceleration. Technical Memorandum 96-3, Naval Aerospace Medical Research Laboratory, Pensacola Fa

Graaf B de, Bos JE, Groen E, Tielemans W, Rameckers F, Clark JB, Mead AM, Guedry FE (1998) Otolith responses during centrifugation along three axes of orientation. Report 1402, Naval Aerospace Medical Research Laboratory, Pensacola, Fa

Graybiel A, Brown RH (1951) The delay in visual reorientation following exposure to a change in direction of resultant force on a human centrifuge. J Gen Psychol 45: 143–150

Graybiel A, Clark B (1965) Validity of the oculogravic illusion as a specific indicator of otolith function. Aerospace Med 36: 1173–1181

Graybiel A, Clark B, MacCorquodale K (1947) The illusory perception of movement caused by angular acceleration and centrifugal force during flight. I. Methodology and preliminary results. J Exp Psychol 37: 170–177

Guedry FE (1974) Psychophysics of vestibular sensation. In Kornhuber HH (ed) The vestibular system part 2: psychophysics, applied aspects and general interpretations. (Handbook of sensory physiology, vol VI/2) Springer, Berlin Heidelberg New York 31–54

Helmholtz H von (1866) Handbuch der Physiologische Optik. Voss, Leipzig

Holly JE (1997) Three-dimensional baselines for perceived self-motion during acceleration and deceleration in a centrifuge. J Vestib Res 7: 45–61

Holst E von, Mittelstaedt H (1950) Das Reafferenzprinzip. Naturwissenschaften 37: 464–476

Howard IP (1986) The vestibular system. In Boff KR, Kaufman L, Thomas JP (eds), Sensory processes and perception. Handbook of perception and human performance, vol 1 1. Wiley, New York, pp 11.1–11.30

Howard IP (1997) Interactions within and between the spatial senses. J Vestib Res 7: 311–345

Kornhuber HH (1974) Introduction. In Kornhuber HH (ed), The vestibular system part 1: basic mechanisms. (Handbook of sensory physiology, Vol VI/1) Springer, Berlin Heidelberg New York 3–14

Lackner JR, Graybiel A (1978) Postural illusions experienced during z-axis recumbent rotation and their dependence upon somatosensory stimulation of the body surface. Aviat Space Environ Med 49: 484–488

Lindeman HH (1973) Anatomy of the otolith organs. Adv Otorhinolaryngol 20: 405–433

Lowenstein O, Sand A (1940) The mechanism, of the semicircular canal. A study of the responses of singlefiber preparations to angular accelerations and to rotation at constant speed. Proc R Soc Lond B 129: 256–275

Mach E (1898) On sensations of orientation. In: McCormack TJ (transl) (ed) Popular scientific lectures, 3rd edn. Open Court, Chicago; pp 282–308

Mayne R (1974) A systems concept of the vestibular organs. In: Kornhuber HH (ed) Handbook of Sensory Physiology, vol VI. Vestibular System Part 2: Psychophysics, Applied Aspects and General Interpretations. Springer, Berlin Heidelberg New York pp 493–580

McCauley ME, Royal JW, Wylie CD, O'Hanlon JF, Mackie RR (1976) Motion sickness indidence: exploratory studies of habituation, pitch and roll, and the refinement of a mathematical model. Technical Report 1733–2, Human Factors Research Inc., Goleta, Calif.

Medendorp WP, Melis BJM, Gielen CCAM, van Gisbergen JAM (1998) Off-centric rotation axes in natural head movements: implications for vestibular reafference and kinematic redundancy. J Neurophysiol 79: 2025–2039

Merfeld DM (1995) Modeling the vestibulo-ocular reflex of the squirrel monkey during eccentric rotation and roll tilt. Exp Brain Res 106: 123–134

Merfeld DM, Young LR, Oman CM, Shelhamer MJ (1993) A multidimensional model of the effect of gravity on the spatial orientation of the monkey. J Vestib Res 3: 141–161

Merfeld DM, Zupan L, Peterka RJ (1999) Humans use internal models to estimate gravity and linear acceleration. Nature 398: 615–618

Merfeld DM, Zupan LH, Gifford CA (2001) Neural processing of gravito-inertial cues in humans. II. Influence of the semicircular canals during eccentric rotation. J Neurophysiol 85: 1648–1660

Mergner T, Glasauer S (1999) A simple model of vestibular canal-otolith signal fusion. Ann N Y Acad Sci 871: 430–434

Mittelstaedt H (1975) On the processing of postural information. Fortschr Zool 23: 128–141

Mittelstaedt H (1983) A new solution to the problem of the subjective vertical. Naturwissenschaften 70: 272–281

Mittelstaedt H (1988) The information processing structure of the subjective vertical. A cybernetic bridge between its psychophysics and its neurobiology. In: Marko H, Hauske G, Struppler A (eds) Processing of structures for perception and action. VCH, Weinheim, pp 217–263

Mittelstaedt H (1992) Somatic versus vestibular gravity reception in man. Ann N Y Acad Sci 656: 124–139

Mittelstaedt H, Fricke E (1988) The relative effect of saccular and somatosensory information on spatial perception and control. Adv Otorhinolaryngol 42: 24–30

Mittelstaedt H, Glasauer S, Gralla G, Mittelstaedt ML (1989) How to explain a constant subjective vertical at constant high speed rotation about an earthhorizontal axis. Acta Otolaryngol Suppl 468: 295–299

Muller M (1990) Relationships between semicircular duct radii with some implications for time constants. Neth J Zool 40: 173–202

Okada T, Grunfeld E, ShalloHoffmann J, Bronstein AM (1999) Vestibular perception of angular velocity in normal subjects and in patients with congenital nystagmus. Brain 122: 1293–1303

Oman CM (1982) A heuristic mathematical model for the dynamics of sensory conflict and motion sickness. Acta Otolaryngol Suppl 392: 1–44

Paige GD, Tomko DL (1991) Eye movement responses to linear head motion in the squirrel monkey. I. Basic characteristics. J Neurophysiol 65: 1170–1182

Purkinje J (1820) Beitrage zur naheren Kenntiniss des Schwindels aus herautognostischen Daten. Wien: Medicinistische Jahrbucher des kaiserl konigl osterreichischen Staates. 4: 79–125

Raphan T, Matsuo V, Cohen B (1979) Velocity storage in the vestibulo-ocular reflex arc (VOR). Exp Brain Res 35: 229–248

Reason JT, Brand JJ (1975) Motion sickness. Academic, London

Robinson DA (1977) Linear addition of optokinetic and vestibular signals in the vestibular nucleus. Exp Brain Res 30: 447–450

Seidman SH, Telford L, Paige GD (1998) Tilt perception during dynamic linear acceleration. Exp Brain Res 119: 307–314

Steinhausen W (1931) Ueber den Nachweis der Bewegung der Cupula in der intakten Bogengangsampulle des Labyrinthes bei der naturlichen rotatorischen und calorischen Reizung. Pflugers Arch Physiol 228: 322–328

Steinhausen W (1933) Ueber die Beobachtung der Cupula in den Bogengangsampullen des Labyrinths des lebenden Hechts. Pflugers Arch 232: 500–512

Stratton GM (1896) Vision without inversion of the retinal image. Psychol Rev 3: 611–617

Stockwell CW, Guedry FE (1970) The effect of semicircular canal stimulation during tilting on the subsequent perception of the visual vertical. Acta Otolaryngol 70: 170–175

Telford L, Seidman SH, Paige GD (1997) Dynamics of squirrel monkey linear vestibuloocular reflex and interactions with fixation distance. J Neurophysiol 78: 1775–1790

Tweed D, Fetter M, Sievering D, Misslisch H, Koenig E (1994a) Rotational kinematics of the human vestibulo-ocular reflex. II. Velocity steps. J Neurophysiol 72: 2480–2489

Tweed D, Sievering D, Misslisch H, Fetter M, Zee D, Koenig E (1994b) Rotational kinematics of the human vestibulo-ocular reflex. I. Gain matrices. J Neurophysiol 72: 2467–2479

Tweed D, Vilis T (1987) Implications of rotational kinematics for the oculomotor system in three dimensions. J Neurophysiol 58: 832–849

Viéville T, Faugeras OD (1990) Cooperation of the inertial and visual systems. In: Henderson TC (ed) Traditional and non-traditional robotic sensors. Springer, Berlin Heidelberg New York, pp 339–350

Wertheimer M (1912) Experimentelle Studien ueber das Sehen von Bewegung. Zsch Psychol 61: 161–265

Westheimer G (1957) Kinematics of the eye. J Opt Soc Am 47: 967–974

Young LR, Meiry JL (1968) A revised dynamic otolith model. Aerosp Med 39: 606–608